R. & M. No. 2960
(16,817)
A.R.C. Technical Report

MINISTRY OF SUPPLY

AERONAUTICAL RESEARCH COUNCIL
REPORTS AND MEMORANDA

Theoretical Load Distribution on a Wing with Vertical Plates

By

J. WEBER, DR.RER.NAT.

LONDON: HER MAJESTY'S STATIONERY OFFICE

1956

PRICE 11*s* 6*d* NET

Theoretical Load Distribution on a Wing with Vertical Plates

By

J. WEBER, DR.RER.NAT.

Reports and Memoranda No. 2960*

March, 1954

Summary.—The spanwise load distribution is calculated for wings with plates normal to the wing and parallel to the main stream, or inclined to it at a small angle. The calculations are made for configurations having minimum induced drag. The results are used to obtain an approximation for wings of any plan-form (where the condition of minimum induced drag no longer applies), including wings with sweepback.

Wings with plates of equal height on the upper and lower surfaces of the wing, and wings with plates on the upper surface only, are considered. Charts and tables for the additional load distribution with plates of various heights, $0 < h/b < 0{\cdot}3$, at the spanwise positions: $b_1/b = 0{\cdot}2, 0{\cdot}4, 0{\cdot}6, 0{\cdot}8, 0{\cdot}9, 1{\cdot}0$ are given. Side-force distributions on the plates, as well as integrated side-forces and the moments of the side-force, are calculated.

In the Appendix, a method of calculating the load distribution on wings with a discontinuity in chord, sectional lift slope, or geometric incidence is described.

1. *Introduction.*—This report considers the case of thin wings, with or without sweep, with two plates placed symmetrically about the centre-line at any given spanwise station. The plates are normal to the wing surface, and parallel or nearly parallel to the main flow (*see* Fig. 1).

A study of the flow around wings with plates has been previously made mainly with a view to its application to tailplane arrangements with twin fins. In this case the height of the vertical plates is of the same order as the span of the wing. More recently, similar plates have been used as ' fences ' to improve the pitching-moment behaviour of swept wings; in this case, the height of the plates is much smaller than the wing span. Mangler's end-plate theory[1] was developed for application to fin-tail arrangements and is not particularly suitable for fences, or other plates of small height. A simpler method of calculation is obtained in a different way for the case of symmetrical wing-plate arrangement, *i.e.*, where the plates are of equal height above and below the wing. This report also gives results for plates on the upper surface only.

Vertical plates added to a wing alter the spanwise load distribution because the system of trailing vortices is modified. Trailing vortices are shed from the plates as well as from the wing. In the case of minimum induced drag, which forms the basis of the present method, a cross-section through the wake has the same shape as a cross-section through the wing-plate configuration itself. Such a wake produces a downwash field which differs from that of the wing alone, so the vortex distribution over the wing and in the wake, and therefore the wing load, must be rearranged to meet the given boundary conditions.

Fences on swept wings also affect the chordwise loading owing to the partial reflection effect which they exercise on the bound vortices, as has been pointed out in Ref. 2. It will be shown below—and this is supported by the experimental evidence given in Ref. 3—that the change in

* R.A.E. Report Aero. 2500—received 31st May, 1954.

spanwise loading, which is caused by fences, is associated mainly with the particular shape of the wake and its associated downwash field. This implies that the results given in this report should lead to a reasonably good approximation for the spanwise loading. The chordwise loading and the pressure distribution over the surface of the wing must subsequently be determined by taking account of the reflection effect.

The theory given in this report also offers a possible step in the calculation of the effect of part-span vortex sheets which exist on wings with different types of flow along the span (*see* Ref. 2). This is a much more difficult problem because the shape of the vortex sheet is not known and has to be determined from the condition that it cannot sustain any forces. However, the trailing vortices in the Trefftz-plane behind the wing are probably very like those produced by solid plates and the method given here can be used to calculate the downwash field from such trailing vortex sheets. With this possible application in mind plates of greater height than those normally used as fences have been included in the calculated examples.

The load distributions are calculated for arrangements giving minimum induced drag, *i.e.*, for configurations producing such systems of trailing vortices as induce a constant downwash along the span and zero sidewash along the plates. The problem then reduces to an investigation of flow in the Trefftz-plane, around simple geometric configurations as shown in Fig. 1. In the case of plates of equal height above and below the wing, the calculation has been considerably simplified by using a conformal transformation of the Trefftz-plane proposed by Betz[4]. Because of this different approach, and to simplify matters for the reader, the method of calculation is explained in full, no detailed reference being made to Mangler's work[1].

The results obtained by using configurations with minimum induced drag can be used to obtain an estimate for the additional load distribution caused by plates on any wing, where the induced drag is not a minimum. In addition to the load distribution on the wing, the side-force distribution on the plates and the moment of the side-force are calculated. The present report does not give any comparison with experimental results (but *see* Ref. 3 for the case of fences on a swept-back wing).

In the appendix, Multhopp's method for calculating the load distribution over a wing alone is extended to include wings with a discontinuity in incidence, chord or sectional lift slope. This method, which was suggested for straight wings by I. Weissinger[5,6] can also be applied to the case of a swept wing. Such discontinuities occur, for instance, when the reflection effect of fences is considered, and the sectional lift slopes on either side of the fence are therefore different.

The method is presented for incompressible flow only. It can easily be applied to subcritical compressible flow by means of the Prandtl-Glauert analogy (*see, e.g.*, Ref. 7), within the limitations of that theory.

2. *Plates of Equal Height Above and Below the Wing.*—2.1. *The Potential Function in the Trefftz-plane.*—The load distribution over the wing and the distribution of the side-forces over the plates are determined from the difference of the potential function on the two surfaces of the vortex sheet far down stream (*i.e.*, in the so-called Trefftz-plane). The induced drag is assumed to be a minimum and it is assumed that the wake does not change its shape and moves downwards with the constant velocity $v_{z\,\infty}$. In this case, the problem reduces to determining the two-dimensional flow in the Trefftz-plane around the wake contour which has the shape of a cross-section through the wing and plates, *see* Fig. 1. The flow around the contour of the moving wake can be determined as the flow around the contour of the fixed wake in a parallel stream of velocity $-v_{z\,\infty}$, superimposed upon a parallel flow of velocity $v_{z\,\infty}$.

The flow around the contour of the fixed wake will be found by a series of conformal transformations. The case of plates of equal height above and below the wing is dealt with separately, since we use transformations different from those for plates above the wing only. The present method, which was suggested by A. Betz[4], makes use of the symmetry of the wake with regard to the wing plane and leads to simple relations.

A rectangular co-ordinate system x, y, z is chosen with x along wind, y spanwise, z positive downwards and the origin at the point of symmetry of the wake contour (*see* Fig. 2). All linear dimensions are referred to the wing semispan ($b/2 = 1$). The spanwise distance between the plates is b_1, their total height h. For simplicity we call the traces of the wing and the plates in the wake simply the wing and the plates.

To determine a flow which satisfies the boundary condition of zero velocity normal to the fixed wake contour, the contour is transformed into a slit along the vertical axis in the ζ_4-plane. This transformation is done in several steps. Advantage is taken of the symmetry of the wake about the z-axis to transform the right half of the ζ-plane ($y > 0$)

$$\zeta = z + iy \qquad \text{(2–1)}$$

into the full ζ_1-plane

$$\zeta_1 = z_1 + iy_1 \qquad \text{(2–2)}$$

by the transformation

$$\zeta_1 = -i\zeta^2 . \qquad \text{(2–3)}$$

With this transformation the wing remains a straight line and the plate becomes an arc of a parabola. Then this parabola is replaced by an arc of a circle through the points B_1, C_1, G_1, in the ζ_1-plane which correspond to B, C, G in the ζ-plane, *see* Fig. 2. This means that the original straight plates are replaced by slightly curved ones; this has a negligible effect for the small plates in which we are interested. This can be seen by comparing the results given in Ref. 8 for straight end-plates with those obtained by the present method for end-plates which are slightly curved so as to give a circular arc in the ζ_1-plane. The difference between the curved plates and the assumed straight plates decreases with increasing spanwise distance $b_1/2$ and decreasing height h of the plates. A few values of the maximum difference $y - b_1/2$ are given below to illustrate that the effect is small:

$b_1/2$	$h/2$	$(y - b_1/2)_{\max.}$
0·2	0·2	0·0040
0·6	0·2	0·0002
0·6	0·4	0·0030
1·0	0·4	0·0007

The co-ordinates of certain interesting points along the wake in the various planes of transformation are listed in Table 1.

In the next step the arc of the circle through the points C_1, B_1, G_1 is transformed into a full circle, whilst the wing remains a straight line. This transformation is given by the relation

$$\zeta_1 - iy_{C_1} = \zeta_2 + \frac{z_{C_1}^2}{4} \cdot \frac{1}{\zeta_2}$$

hence

$$\zeta_2 = \tfrac{1}{2}\left\{\zeta_1 - i\left[\left(\frac{b_1}{2}\right)^2 - \left(\frac{h}{2}\right)^2\right] \pm \sqrt{\left[\left\{\zeta_1 - i\left[\left(\frac{b_1}{2}\right)^2 - \left(\frac{h}{2}\right)^2\right]\right\}^2 - \left(\frac{hb_1}{2}\right)^2\right]}\right\} . \qquad \text{(2–4)}$$

The centre of the circle is

$$\zeta_2 = i \cdot \tfrac{1}{2}\left(\frac{h}{2}\right)^2$$

and the radius

$$= \tfrac{1}{2}\sqrt{\left[\left(\frac{hb_1}{2}\right)^2 + \left(\frac{h}{2}\right)^4\right]} .$$

Next, the circle and the straight line corresponding to the wing are transformed into a slit along the y_3-axis:

$$\zeta_3 = \zeta_2 - i \cdot \tfrac{1}{2}\left(\frac{h}{2}\right)^2 - \tfrac{1}{4}\frac{\left(\frac{hb_1}{2}\right)^2 + \left(\frac{h}{2}\right)^4}{\zeta_2 - i \cdot \tfrac{1}{2}\left(\frac{h}{2}\right)^2} \quad \ldots\ldots\ldots\ldots\ldots\ldots \quad (2\text{–}5)$$

Finally, the full slitted ζ_3-plane is transformed into the right half of the ζ_4-plane by the transformation

$$\zeta_4 = \sqrt{[i(\zeta_3 - \zeta_{E_3})]} = \sqrt{[i\zeta_3 + e_3]} \quad \ldots\ldots\ldots\ldots\ldots\ldots \quad (2\text{–}6)$$

where

$$e_3 = e_2 - \tfrac{1}{2}\left(\frac{h}{2}\right)^2 + \tfrac{1}{4}\frac{\left(\frac{hb_1}{2}\right)^2 + \left(\frac{h}{2}\right)^4}{e_2 - \tfrac{1}{2}\left(\frac{h}{2}\right)^2} \quad \ldots\ldots\ldots\ldots\ldots\ldots \quad (2\text{–}7)$$

$$e_2 = \tfrac{1}{2}\left\{1 - \left(\frac{b_1}{2}\right)^2 + \left(\frac{h}{2}\right)^2 + \sqrt{\left[\left\{1 - \left(\frac{b_1}{2}\right)^2 + \left(\frac{h}{2}\right)^2\right\}^2 + \left(\frac{hb_1}{2}\right)^2\right]}\right\} \quad \ldots\ldots \quad (2\text{–}8)$$

Corresponding points on the wing surface, $\zeta = iy$, and the z_4-axis are given by the relations:

$$y_1 = y^2 \quad \ldots\ldots\ldots\ldots\ldots\ldots \quad (2\text{–}9)$$

$$y_2 = \tfrac{1}{2}\left\{y_1 - \left(\frac{b_1}{2}\right)^2 + \left(\frac{h}{2}\right)^2 \pm \sqrt{\left[\left\{y_1 - \left(\frac{b_1}{2}\right)^2 + \left(\frac{h}{2}\right)^2\right\}^2 + \left(\frac{hb_1}{2}\right)^2\right]}\right\} \quad \ldots\ldots \quad (2\text{–}10)$$

with

$$y_2 < 0 \text{ for } 0 < y < \frac{b_1}{2}$$

$$y_2 > 0 \text{ for } \frac{b_1}{2} < y < 1$$

$$y_3 = y_2 - \tfrac{1}{2}\left(\frac{h}{2}\right)^2 + \tfrac{1}{4}\frac{\left(\frac{hb_1}{2}\right)^2 + \left(\frac{h}{2}\right)^4}{y_2 - \tfrac{1}{2}\left(\frac{h}{2}\right)^2} \quad \ldots\ldots\ldots\ldots\ldots\ldots \quad (2\text{–}11)$$

$$z_4 = \mp \sqrt{[e_3 - y_3]} \cdot \quad \ldots\ldots\ldots\ldots\ldots\ldots \quad (2\text{–}12)$$

As stated above, the straight plates have been replaced by slightly curved ones. If points with the same z-co-ordinate are correlated, then we find corresponding points on the plates and the z_4-axis by the relations:

$$\sqrt{\left\{e_3 - \sqrt{\left[\left(\frac{hb_1}{2}\right)^2 + \left(\frac{h}{2}\right)^4\right]}\right\}} < |z_4| < \sqrt{\left\{e_3 + \sqrt{\left[\left(\frac{hb_1}{2}\right)^2 + \left(\frac{h}{2}\right)^4\right]}\right\}}$$

$$y_3 = e_3 - z_4^2 \quad \ldots\ldots\ldots\ldots\ldots\ldots \quad (2\text{–}13)$$

$$z_2 = \pm \tfrac{1}{2}\sqrt{\left[\left(\frac{hb_1}{2}\right)^2 + \left(\frac{h}{2}\right)^4 - y_3^2\right]} \quad \ldots\ldots\ldots\ldots\ldots\ldots \quad (2\text{–}14)$$

$$z_1 = z_2\left[1 + \frac{\left(\frac{b_1}{2}\right)^2}{\left(\frac{b_1}{2}\right)^2 + \frac{1}{2}\left(\frac{h}{2}\right)^2 + \frac{1}{2}y_3}\right] \quad \ldots\ldots\ldots\ldots\ldots\ldots \quad (2\text{–}15)$$

$$z = \tfrac{1}{2}\frac{z_1}{b_1/2} \cdot \quad \ldots\ldots\ldots\ldots\ldots\ldots \quad (2\text{–}16)$$

At large distances away from the wake contour, *i.e.*, for $\zeta \to \infty$,

$$\zeta_1 = \zeta_2 = \zeta_3 \quad .. \quad .. \quad .. \quad .. \quad .. \quad .. \quad .. \quad .. \quad (2\text{–}17)$$

and

$$\zeta_4 = \sqrt{(i\zeta_1)} = \zeta \quad .. \quad .. \quad .. \quad .. \quad .. \quad .. \quad .. \quad (2\text{–}18)$$

This means that the parallel flow with velocity $-v_{z\infty}$ in the ζ-plane corresponds to a parallel flow with the same velocity in the ζ_4-plane. In the ζ_4-plane the transform of the wake is a vertical plate, which does not present an obstacle to the parallel flow, and we are left with parallel flow everywhere. The complex potential $F_1(\zeta)$ of the flow around the fixed wake contour is therefore:

$$F_1(\zeta) = \phi_1(z,y) + i\psi_1(z,y) = -v_{z\infty}\zeta_4(\zeta)\frac{b}{2} \quad .. \quad .. \quad .. \quad .. \quad (2\text{–}19)$$

and the total potential for the moving wake is:

$$F(\zeta) = F_1(\zeta) + v_{z\infty}\zeta\frac{b}{2} = -v_{z\infty}\left[\zeta_4(\zeta) - \zeta\right]\frac{b}{2}. \quad .. \quad .. \quad .. \quad (2\text{–}20)$$

The potential for points on the wing or the plates is thus

$$\phi(z,y) = -v_{z\infty}\left[z_4(z,y) - z\right]\frac{b}{2} \quad .. \quad .. \quad .. \quad .. \quad .. \quad .. \quad (2\text{–}21)$$

where $z_4(z,y)$ is to be calculated by equations (2–9) to (2–16).

2.2. *The Load Distribution on the Wing.*—The local lift coefficient on the wing is related to the difference of the potential function on the upper and lower surfaces of the vortex sheet in the Trefftz-plane by

$$C_L = \frac{2}{cV_0}(\phi_{US} - \phi_{LS}) \quad .. \quad .. \quad .. \quad .. \quad .. \quad .. \quad .. \quad (2\text{–}22)$$

where c is the local wing chord, used as reference chord for the local lift coefficient C_L, and V_0 is the velocity of the main flow.

We obtain from equation (2–21)

$$C_L(y) \cdot c(y) = 4\frac{v_{z\infty}}{V_0}|z_4(y)|\frac{b}{2}. \quad .. \quad .. \quad .. \quad .. \quad .. \quad .. \quad (2\text{–}23)$$

The coefficient $\bar{C}_L$ of the overall lift over the wing is obtained by integration. $\bar{C}_L$ is referred to the wing area $b\bar{c}$, where $\bar{c}$ is the mean wing chord. It is

$$\begin{aligned}\bar{C}_L &= \int_0^1 C_L(y)\frac{c(y)}{\bar{c}}\,d\left(\frac{y}{b/2}\right) \\ &= A \cdot \frac{v_{z\infty}}{V_0} I \quad .. \quad .. \quad .. \quad .. \quad .. \quad .. \quad .. \quad (2\text{–}24)\end{aligned}$$

where

$$A = \frac{b}{\bar{c}}$$

is the aspect ratio of the wing, and

$$I = 2\int_0^1 |z_4(y)|\,d\left(\frac{y}{b/2}\right). \quad .. \quad .. \quad .. \quad .. \quad .. \quad .. \quad (2\text{–}25)$$

I is a function of h/b and b_1/b but is independent of the aspect ratio.

The shape of the spanwise load distribution is given by the relation

$$\frac{C_L(y) \cdot c(y)}{\bar{C}_L\bar{c}} = \frac{2|z_4(y)|}{I}. \quad .. \quad .. \quad .. \quad .. \quad .. \quad .. \quad .. \quad (2\text{–}26)$$

Again, this is only a function of h/b and b_1/b. A few examples are given in Fig. 3.

To determine the actual load requires a knowledge of the total lift coefficient $\bar{C}_L$ which is determined by equations (2–24) and (2–25) except for the factor $v_{z\infty}/V_0$. The next task is, therefore, to determine the downwash velocity $v_{z\infty}/V_0$. This is done by relating the conditions in the wake to those on the wing.

The local lift coefficient is equal to the sectional lift slope $a(y)$, as defined in Ref. 7, multiplied by the effective incidence α_e, which is equal to the geometric incidence α reduced by the induced incidence α_i:

$$\frac{C_L(y)}{\alpha} = a(y)\frac{\alpha_e}{\alpha} = a(y)\left[1 - \frac{\alpha_i}{\alpha}\right]. \qquad \text{(2–27)}$$

The incidence α_i which the trailing vortices induce at the wing is proportional to the downwash far downstream:

$$\alpha_i = \frac{v_z}{V_0} = \frac{\omega}{2}\frac{v_{z\infty}}{V_0}. \qquad \text{(2–28)}$$

The value of ω depends mainly on the aspect ratio of the wing; $\omega = 1$ for wings of large aspect ratio and $\omega = 2$ for $A \to 0$. A method for calculating ω has been given by D. Küchemann[7]. The problem is now reduced to finding α_i, which depends on the plan-form and sectional properties of the wing.

The sectional lift slope $a(y)$ is a function of the aspect ratio and, for swept wings, of the angle of sweep and the spanwise position (*see* Ref. 7). Plates on a swept wing have a further effect on the load distribution besides the one on the trailing vortices. They act on the bound vortices as partial reflection plates and change the chordwise load distribution (*see* Refs. 2 and 3) and hence the sectional lift slope. Plates on a swept-back wing increase $a(y)$ inboard of the plate as in the centre-section of a swept-forward wing and reduce it outboard of the plate. What percentage of the full reflection effect of a large plate is achieved by a small plate depends on the height of the plate and the chordwise extent (*see* Ref. 3).

Since we consider wing-plate arrangements which produce a constant induced incidence and thus a constant effective incidence along the span, it follows from equation (2–27) that the spanwise variation of the sectional lift slope means that the local lift coefficient $C_L(y)$ varies along the span. Only for unswept wings does $C_L(y) = \bar{C}_L$. The spanwise load distribution, as given by equation (2–26), does not depend on the sweep of the wing, which means that the minimum induced drag configuration must have a chord distribution which depends on the angle of sweep and the aspect ratio of the wing. The chord distribution can be determined by combining equations (2–23), (2–27) and (2–28):

$$\frac{c(y)}{b/2} = \frac{8}{\omega}\frac{\alpha_i/\alpha}{1 - (\alpha_i/\alpha)}\frac{|z_4(y)|}{a(y)}. \qquad \text{(2–29)}$$

For unswept wings, by equations (2–26) and (2–29):

$$\frac{c(y)}{\bar{c}} = \frac{|z_4(y)|}{I/2}. \qquad \text{(2–30)}$$

For swept wings, where a is a function of y,

$$\frac{c(y)}{\bar{c}} = \frac{\dfrac{|z_4(y)|}{a(y)}}{\displaystyle\int_0^1 \frac{|z_4(y)|}{a(y)}\, d\left(\frac{y}{b/2}\right)}. \qquad \text{(2–31)}$$

Integrating $c(y)$ of equation (2–29) along the span gives the required relation for the unknown α_i/α if the values of A, ω, $a(y)$, h/b, b_1/b are known:

$$\int_0^1 \frac{c(y)}{b/2}\, d\left(\frac{y}{b/2}\right) = \frac{\bar{c}}{b/2} = \frac{2}{A}$$

$$= \frac{8}{\omega}\frac{\alpha_i/\alpha}{1-(\alpha_i/\alpha)} \cdot \int_0^1 \frac{|z_4(y)|}{a(y)}\, d\left(\frac{y}{b/2}\right)$$

$$\frac{\alpha_i/\alpha}{1-(\alpha_i/\alpha)} = \frac{\omega}{4A}\frac{1}{\int_0^1 \frac{|z_4(y)|}{a(y)}\, d\left(\frac{y}{b/2}\right)} \quad \ldots\ldots\ldots\ldots\ldots\ldots \quad (2\text{–}32)$$

When α_i is known the downwash at infinity can be determined by equation (2–28), and thence the overall lift slope from equation (2–24), which gives

$$\frac{\bar{C}_L}{\alpha} = \frac{2}{\omega}\frac{\alpha_i}{\alpha} AI\,. \quad \ldots\ldots\ldots\ldots\ldots\ldots \quad (2\text{–}33)$$

The difficulty lies in finding the value of $a(y)$, and therefore the value of the integral in equation (2–32). The spanwise variation of $a(y)$ can be taken into account correctly by an iteration process. The sectional lift slope a is a function of the distances from the centre, the tip and the plates, measured in terms of the local chord $c(y)$. $c(y)$ can be determined by equation (2–31), assuming a first approximation of $a(y)$; with the known $c(y)$ new values of $a(y)$ can be found.

A simplified though only approximate formula for α_i/α can be found. By definition

$$\frac{\bar{C}_L}{\alpha} = \int_0^1 \frac{C_L(y)}{\alpha}\frac{c(y)}{\bar{c}}\, d\left(\frac{y}{b/2}\right)$$

$$= \left(1-\frac{\alpha_i}{\alpha}\right)\int_0^1 a(y)\frac{c(y)}{\bar{c}}\, \mathrm{d}\left(\frac{y}{b/2}\right) \quad \ldots\ldots\ldots\ldots \quad (2\text{–}34)$$

which again contains the unknown $a(y)$. The sectional lift slope on a swept wing near mid-semispan is that of the corresponding two-dimensional sheared wing a_s; at the centre the value is smaller than a_s and at the tips it is larger. The increase of the sectional lift slope near the tips is usually greater than the decrease near the centre. This difference is reduced by the greater values of $c(y)/\bar{c}$ at the centre for the ordinary tapered wings. The reflection effect of the plates causes a change in the sectional lift slope which is of opposite sign inboard and outboard of the plate, so whenever there is a spanwise position at which a is greater than a_s, there is also another at which a is less than a_s. A reasonable approximation is therefore

$$\int_0^1 a(y)\frac{c(y)}{\bar{c}}\, d\left(\frac{y}{b/2}\right) = a_s = a_0 \cos\varphi \quad \ldots\ldots\ldots\ldots \quad (2\text{–}35)$$

where a_0 is the two-dimensional lift slope of the aerofoil section ($a_0 = 2\pi$ for a thin flat plate). With this approximation, we obtain by equations (2–33) and (2–34)

$$\frac{\alpha_i/\alpha}{1-(\alpha_i/\alpha)} = \frac{\omega a_s}{2AI}$$

and

$$\frac{\alpha_i}{\alpha} = \frac{\frac{\omega a_s}{2AI}}{1+\frac{\omega a_s}{2AI}}\,. \quad \ldots\ldots\ldots\ldots \quad (2\text{–}36)$$

This is an approximation to equation (2–32), and is the same as that obtained by replacing $a(y)$ by a_s in equation (2–32). This means that for unswept wings equation (2–36) is exactly true. The overall lift slope is given by equations (2–33) and (2–36):

$$\frac{\bar{C}_L}{\alpha} = \frac{a}{1 + \varkappa \frac{\omega a}{\pi A}} \qquad \text{(2–37)}$$

with

$$a = a_s$$

$$\varkappa = \frac{\pi}{2I}. \qquad \text{(2–38)}$$

Equation (2–37) is similar to Prandtl's well-known relation for wings with elliptic span loading, extended to include wings of small aspect ratio, *see* Ref. 7, where the effect of the plates is taken into account by $\varkappa$. Calculated $\varkappa$-values are plotted in Fig. 4.

The factor $\varkappa$ also gives the reduction of the induced drag of the wing with plates as compared with the induced drag of the wing without plates:

$$\bar{C}_{Di} = \tfrac{1}{2} \frac{v_{z\infty}}{V_0} \bar{C}_L = \frac{\alpha_i}{\omega} \bar{C}_L$$

$$= \varkappa \frac{\bar{C}_L^2}{\pi A}. \qquad \text{(2–39)}$$

Finally, we estimate the effect of plates on the spanwise load distribution of wings of any plan-form. A simple approximation is obtained by subtracting from the load distribution of the minimum induced drag configuration the load distribution of the wing without plates which has minimum induced drag, and which has the same A, ω and a. This procedure is not strictly correct since the plan-forms of the wing with plates and the wing alone differ from one another, but it has been proved to give a reasonable estimate in similar cases.

The spanwise distribution of the additional load is:

$$\frac{\Delta C_L(y)}{\alpha} \frac{c(y)}{\bar{c}} = \frac{\bar{C}_L}{\alpha} \frac{C_L c}{\bar{C}_L \bar{c}} - \frac{\bar{C}_{L0}}{\alpha} \frac{4}{\pi} \sqrt{\left\{1 - \left(\frac{y}{b/2}\right)^2\right\}}$$

$$= \frac{\bar{C}_L}{\alpha} \left[\frac{C_L c}{\bar{C}_L \bar{c}} - \frac{4}{\pi} \sqrt{\left\{1 - \left(\frac{y}{b/2}\right)^2\right\}}\right]$$

$$+ \frac{\Delta \bar{C}_L}{\alpha} \frac{4}{\pi} \sqrt{\left\{1 - \left(\frac{y}{b/2}\right)^2\right\}} \qquad \text{(2–40)}$$

where $\bar{C}_{L0}$ is the overall lift coefficient for the wing without plates.

The change $\Delta \bar{C}_L/\alpha$ in the overall lift slope due to the plates is given by the relation:

$$\frac{\Delta \bar{C}_L}{\alpha} = \frac{\bar{C}_L}{\alpha} - \frac{\bar{C}_{L0}}{\alpha}$$

$$= \frac{a}{1 + \varkappa \frac{\omega a}{\pi A}} - \frac{a}{1 + \frac{\omega a}{\pi A}}$$

$$= \frac{\bar{C}_{L0}}{\alpha} \left(\frac{1 + \frac{\omega a}{\pi A}}{1 + \varkappa \frac{\omega a}{\pi A}} - 1 \right)$$

$$= (1 - \varkappa) \frac{\omega}{\pi A} \frac{a}{1 + \varkappa \cdot \frac{\omega a}{\pi A}} \cdot \frac{\bar{C}_{L0}}{\alpha} \qquad \text{(2–41)}$$

so that

$$\frac{\Delta \bar{C}_L}{\bar{C}_L} = (1 - \varkappa)\frac{\omega}{\pi A}\frac{\bar{C}_{L0}}{\alpha}. \qquad (2\text{–}42)$$

With small plates at inboard positions $\Delta \bar{C}_L/\alpha$ is small so that the second term in equation (2–40) can be neglected. The function $C_L(y) \cdot c(y)/\bar{C}_L\bar{c}$ is known by equation (2–26).

The difference

$$\frac{C_L c}{\bar{C}_L \bar{c}} - \frac{4}{\pi}\sqrt{\left\{1 - \left(\frac{y}{b/2}\right)^2\right\}} = \frac{2|z_4(y)|}{I} - \frac{4}{\pi}\sqrt{\left\{1 - \left(\frac{y}{b/2}\right)^2\right\}}$$

is plotted in Figs. 5 to 10 and tabulated in Table 2.

To check the accuracy of the additional load distribution given by equation (2–40), one can calculate the load distribution of that wing alone which gives, with the plates, a minimum induced drag configuration. By determining the difference between the load distribution of the wing-plate arrangement of equations (2–26), (2–32) and (2–33) and the load distribution of the wing alone one obtains the exact change in the load distribution caused by adding the plates. We shall do this calculation for a few examples. The height of the plates chosen in the following examples is greater than with fences on practical wings. The greater height shows the effects more clearly since, *e.g.*, the differences in plan-form are increased.

For unswept wings, the chord distribution of the wing which, with the plates added, gives a minimum induced-drag configuration, is given by equation (2–30). With $z_4(D_4) \neq z_4(B_4)$ (*see* Fig. 2) this plan-form has a discontinuity at the position of the plate. This discontinuity produces a discontinuity in the induced incidence which means that it cannot be determined by the usual methods. I. Weissinger[5, 6] has extended the method of H. Multhopp for calculating the load distribution over wings with a discontinuity in the geometric incidence to cover wings with a discontinuity in the chord. The same procedure can be applied if there is a discontinuity in the sectional lift slope $a(y)$. The method is described in the Appendix.

For the unswept wing of aspect ratio 4 which, with two symmetrical plates of height $h = 0{\cdot}2b$ at $y = \pm\, 0{\cdot}6b/2$, gives a minimum induced drag configuration (*see* Fig. 11) the load distribution has been calculated by this method taking $a = 2\pi$, $\omega = 1$. The overall lift slope $\bar{C}_{L0}/\alpha$ of the wing is $4{\cdot}16$ whilst the approximation of equation (2–37) gives for the wing alone $\bar{C}_{L0}/\alpha = 4{\cdot}19$. With $\varkappa = 0{\cdot}960$ from Fig. 4, we get by equation (2–37) a total lift slope $\bar{C}_L/\alpha = 4{\cdot}25$ for the wing-plate arrangement. This is also the exact value, since equation (2–37) is exactly true for minimum induced-drag configurations of unswept wings where the sectional lift slope is constant. Following the proposed approximate procedure, we obtain by equation (2–41) a $\Delta \bar{C}_L/\alpha = 0{\cdot}06$. Adding this value to the lift slope $\bar{C}_{L0}/\alpha$ of the wing alone, in this case equal to $4{\cdot}16$, gives for the total lift slope the approximate value $\bar{C}_L/\alpha = 4{\cdot}22$, *i.e.*, about 1 per cent less than the exact value of $4{\cdot}25$. This error is negligible. The change in the spanwise load distribution which the plates produce is plotted in Fig. 11 together with the approximation of equation (2–40). The comparison shows that equation (2–40) gives an estimate which will be sufficiently accurate in most cases.

With swept wings, the chord distribution of the wing, which with the plates added is a minimum induced drag configuration, varies with the angle of sweep, the magnitude of the reflection effect and the aspect ratio, since these quantities determine the spanwise variation of $a(y)$ (*see* equation (2–31)). The increase of $a(y)$ inboard, and the decrease outboard of the plates due to the reflection effect on swept-back wings counteracts the discontinuity of $z_4(y)$, so that with not too high a reflection effect the discontinuity of the chord is reduced compared with the straight wing. There are cases where the discontinuity in $a(y)$ fully cancels the discontinuity in $z_4(y)$. Such an example is shown in Fig. 12, where the chord distribution of a 45-deg swept-back wing of aspect ratio 4 with plates of height $h = 0{\cdot}2b$ at the spanwise positions $y = \pm\, 0{\cdot}6b/2$ is plotted. The

chord distributions have been calculated for 40 per cent and for full reflection effect. They have been determined under the simplifying assumption that $a(y)$ is a function of $y/\bar{c}$ instead of $y/c(y)$. The chord distribution of the wing with 40 per cent reflection effect does not differ much from the chord distribution of the 45-deg swept-back wing of aspect ratio 4 which is, without plates, a minimum induced-drag wing as shown by the comparison in Fig. 13. In other words, the difference between the plan-forms of the minimum induced-drag configurations of a wing with plates and without plates is less than for the unswept wing (*see* Fig. 11), which further justifies the procedure leading to equation (2–40). A reflection effect of 40 per cent has been measured on a 45-deg swept wing with fences of a size used in practice. For plates with very large reflection effect, the discontinuity of the chord is of opposite sign to that on straight wings.

The load distribution over the wing alone has been calculated for the two chord distributions corresponding to 40 per cent and full reflection effect taking $\omega = 1$ and the sectional lift slope of the two-dimensional wing to be $a_0 = 2\pi$. The overall lift slope of the wing alone corresponding to full reflection (wing I in Fig. 12) is $3{\cdot}18$, for the wing with 40 per cent reflection (wing II in Fig. 12) it is $3{\cdot}20$. The approximate value from equation (2–37) for both wings I and II is $3{\cdot}28$. For the wing with plates the overall lift slope calculated from equations (2–32) and (2–33) for wing I, corresponding to full reflection, is equal to $3{\cdot}28$ and for wing II, corresponding to partial reflection, it is $3{\cdot}25$. The approximate value from equation (2–37) is $3{\cdot}32$ for both wings. By the approximate procedure of calculating $\Delta\bar{C}_L/\alpha$ from equation (2–41), and adding the value to the lift slope of the wing alone, we get for wing I $\bar{C}_L/\alpha = 3{\cdot}22$ and for wing II $\bar{C}_L/\alpha = 3{\cdot}24$ compared with the exact values of $3{\cdot}28$ and $3{\cdot}25$ respectively. In the practical case of a wing with fences, the reflection effect is of the order of 40 per cent of full reflection, in which case the error in the overall lift slope is less than 1 per cent. The exact additional spanwise load distribution has been obtained by subtracting the calculated load distribution of the wing alone from that with the plates present, determined by equation (2–26) and the total lift slope. These distributions are plotted in Fig. 12 together with the approximation resulting from equation (2–40). The approximation is the same for wings I and II. In the extreme case of full reflection equations (2–40) and (2–41) underestimate the plate effect inboard of the plates. With partial reflection, the approximation (2–40) is good inboard. Outboard, equation (2–40) somewhat overestimates the plate effect in all examples considered. With a wing of aspect ratio 4, plates situated inboard of the tips of height $h/b = 0{\cdot}2$, i.e., $h/\bar{c} = 0{\cdot}8$ are for some applications a rather extreme case. It can therefore be concluded that equations (2–41) and (2–40) will give a sufficiently accurate estimate for most practical cases.

As stated above, the change in the spanwise load distribution produced by plates on a swept wing is due to the combined effect of a change of the trailing vortex sheet and the reflection of the bound vortices. To determine the contribution of each of these effects to the total change, we have calculated—by the method given in the Appendix—the load distribution of the wing alone with the discontinuous sectional lift slope distribution of the wing with plates for 40 per cent reflection effect, and subtracted the load distribution of the wing alone calculated with the $a(y)$ distribution of the wing alone. The difference is plotted in Fig. 14 together with the total additional load distribution. This comparison shows that the change in the shape of the trailing vortex sheet is mainly responsible for the additional load distribution. It confirms the assumption made at the beginning that the change in spanwise loading, which is caused by fences, is associated mainly with the particular shape of the wake and the downwash field therefrom. However, the reflection effect does change the chordwise loading.

2.3. *The Side-force on the Plates.*—Some of the bound vortices of the wing continue along the plates. These bound vortices in the main flow of velocity V_0 produce a force normal to the plates. This side-force is directed inwards on the upper part of the plate and outwards on the lower part. The total sum of the side-forces is zero, but they produce a finite moment. In the following, we calculate the distribution of the side-force along the upper half of the plate at $y = b_1/2$, the resultant side-force on the upper part, and the arm of its moment.

The force is proportional to the difference of the potential function between two points of the same height inside and outside the vortex sheet far downstream in the wake; *cf.* equation (2–22):

$$C_Y = \frac{F_Y}{\frac{1}{2}\rho V_0^2 c} = \frac{2}{cV_0}(\phi_{\text{inside}} - \phi_{\text{outside}}) \quad \ldots\ldots\ldots\ldots \quad (2\text{–}43)$$

F_Y is defined to be positive when directed inwards. With equation (2–21):

$$C_Y(z) \cdot c(y) = 2\frac{v_{z\infty}}{V_0}[-z_4(z)_{\text{inside}} - (-z_4(z))_{\text{outside}}]\frac{b}{2} \cdot$$

$$= 2\frac{v_{z\infty}}{V_0}|\Delta z_4(z)|\frac{b}{2}. \quad \ldots\ldots\ldots\ldots \quad (2\text{–}44)$$

From equations (2–13) to (2–16) the function $z(z_4)$ can be calculated and from this one can determine $|\Delta z_4(z)|$ graphically.

Referring the coefficient of the local side-force to the total lift coefficient, as has been done for the local lift coefficient in equation (2–26), we obtain

$$\frac{C_Y c}{\bar{C}_L \bar{c}} = \frac{|\Delta z_4(z)|}{I}. \quad \ldots\ldots\ldots\ldots \quad (2\text{–}45)$$

Side-force distributions are plotted in Fig. 15. We will show in the next section that for plates of small height situated inboard of the tip the distribution of the side-force is elliptic. This is approximately true for plates with $h/b < 0{\cdot}3$.

The total side-force $\bar{F}_Y$ on the upper part of the plate referred to the wing area $b\bar{c}$, is obtained by integration:

$$\bar{C}_Y = \frac{\bar{F}_Y}{\frac{1}{2}\rho V_0^2 b\bar{c}} = A\frac{v_{z\infty}}{V_0} I_Y \quad \ldots\ldots\ldots\ldots \quad (2\text{–}46)$$

where

$$I_Y = \tfrac{1}{2}\int_0^{\frac{1}{2}h/\frac{1}{2}b} |\Delta z_4(z)| \, d\left(\frac{z}{b/2}\right). \quad \ldots\ldots\ldots\ldots \quad (2\text{–}47)$$

The ratio of the side-force $\bar{F}_Y$ to the total lift is therefore

$$\frac{\bar{C}_Y}{\bar{C}_L} = \frac{I_Y}{I}. \quad \ldots\ldots\ldots\ldots \quad (2\text{–}48)$$

This ratio is plotted in Fig. 16.

From the known distribution of the side-force, equation (2–45), both the moment M of the side-force with respect to the plate-wing junction and the arm $z_0 \cdot b/2$ of the side-force can be determined:

$$M = \int_0^{h/2} F_Y z \, dz$$

$$= z_0 \frac{b}{2}\bar{F}_Y \quad \ldots\ldots\ldots\ldots \quad (2\text{–}49)$$

$$z_0 = \frac{\int_0^{\frac{1}{2}h/\frac{1}{2}b} \Delta z_4(z)\frac{z}{b/2}\, d\left(\frac{z}{b/2}\right)}{\int_0^{\frac{1}{2}h/\frac{1}{2}b} \Delta z_4(z)\, d\left(\frac{z}{b/2}\right)}. \quad \ldots\ldots\ldots\ldots \quad (2\text{–}50)$$

z_0 is plotted in Fig. 17. With elliptic side-force distribution,

$$z_0 = \frac{4}{3\pi}\frac{h}{b}. \quad \ldots\ldots\ldots\ldots \quad (2\text{–}51)$$

Fig. 17 shows that equation (2–51) gives a sufficient approximation for all cases considered.

When the system of trailing vortices considered is produced by a wing with solid plates, the plates must be placed at a certain angle to the main flow to produce the required system of bound vortices, and with it the side-force. This has already been pointed out by K. W. Mangler[1].

For unswept wings of not too small an aspect ratio we can assume that the chordwise load distributions inboard and outboard of the plates are those of the two-dimensional wing with the sectional lift slope a. The chordwise side-force distribution on the plate may, however, be different, except for the wing-plate junction. A plate of small height is comparable with a wing of small aspect ratio and it is known (*see* Ref. 7) that the chordwise load distribution of a straight small aspect ratio wing varies with the aspect ratio. It is not possible to determine the distribution of the side-force by assuming that the plate is isolated, since the presence of the wing vortices will affect the vortex distribution on the plate.

With swept wings matters are further complicated by the fact that the chordwise load distribution on the wing is altered by the plate, and in a different manner inboard and outboard of the plate.

To obtain an estimate of the angle between the plate and the direction of the main flow, two extreme cases are now considered. First it is assumed that the chordwise side-force distribution is the same as the load distribution on the wing with the same sectional slope a. In this case, the side-force, integrated along the chord, is a times an effective angle β_e, corresponding to α_e in equation (2–27). Only those arrangements in which the trailing vortex system produces zero v_y-velocity in the wake are considered: this implies that the trailing vortices do not induce a v_y-velocity at the plate. The angle β must therefore be produced by inclining the plate on the upper surface so that the trailing edge of the plate is farther outboard on the wing, by an amount Δy, than the leading edge of the plate:

$$\frac{\Delta y(z)}{c} = \frac{v_y}{V_0} = \frac{1}{a} C_Y(z)$$

$$= \alpha \frac{C_Y c}{\bar{C}_L \bar{c}} \frac{\bar{C}_L/\alpha}{a} \frac{1}{c/\bar{c}} \cdot \quad \ldots \quad \ldots \quad \ldots \quad \ldots \quad \ldots \quad \ldots \quad \ldots \quad (2\text{–}52)$$

$(\bar{C}_L/\alpha)/a$ is known from equation (2–37), and it will be shown in the next section that for small inboard plates

$$\frac{C_Y c}{\bar{C}_L \bar{c}} = \frac{|\Delta z_4(z)|}{I} = \frac{4}{\pi} \frac{b_1/b}{\sqrt{\left\{1 - \left(\frac{b_1}{b}\right)^2\right\}}} \cdot \frac{h}{b} \sqrt{\left\{1 - \left(\frac{z}{h/2}\right)^2\right\}} \cdot \quad \ldots \quad \ldots \quad (2\text{–}53)$$

Hence

$$\frac{\Delta y(z)}{c} = \alpha \frac{h}{b} \sqrt{\left\{1 - \left(\frac{z}{h/2}\right)^2\right\}} \frac{4}{\pi} \frac{b_1/b}{\sqrt{\left\{1 - \left(\frac{b_1}{b}\right)^2\right\}}} \frac{1}{1 + \varkappa \frac{\omega a}{\pi A}} \frac{1}{c/\bar{c}} \cdot \quad \ldots \quad (2\text{–}54)$$

Another estimate is obtained by making the extreme assumption that the chordwise side-force distribution is similar to the load distribution of a small aspect ratio wing, with $A_{\text{plate}} = h/c$. Then for the slope a_{plate} we obtain, *see* Ref. 7:

$$a_{\text{plate}} = 2\pi \sqrt{\left\{\frac{A_{\text{plate}}}{2}\right\}}$$

$$= 2\pi \sqrt{\left\{\frac{A}{2c/\bar{c}}\right\}} \sqrt{\left(\frac{h}{b}\right)} \cdot$$

Using again equation (2–37) and the above approximation for $C_y c/\bar{C}_L \bar{c}$, equation (2–52) gives

$$\frac{\Delta y(z)}{c} = \alpha \sqrt{\left(\frac{h}{b}\right)} \sqrt{\left\{1 - \left(\frac{z}{h/2}\right)^2\right\}} \frac{4}{\pi^2} \frac{b_1/b}{\sqrt{\left\{1 - \left(\frac{b_1}{b}\right)^2\right\}}} \frac{1}{\sqrt{2Ac/\bar{c}}} \frac{a}{1 + \varkappa \frac{\omega a}{\pi A}} \cdot \quad (2\text{–}55)$$

$\Delta y(z)/c$ varies with z in both these expressions, being zero for the top of the plate ($z = h/2$), and greatest at the wing-plate junction. However, the maximum deflection is small for fences in any practical case, and can usually be ignored, so that the calculation can be applied to fences, whether or not they are inclined to the main stream.

2.4. *The Limit $h \to 0$.*—When determining the effect of small plates, as in the case of fences of small height, and when interpolating for heights other than those calculated, it is useful to know the lowest-order term, with respect to h, of the various quantities.

Consider first the case of plates situated inboard of the tip $b_1/2 \neq 1$ and assume:

$$hb_1 << 1 - \left(\frac{b_1}{2}\right)^2$$

$$h^2 << 1 - \left(\frac{b_1}{2}\right)^2.$$

For simplicity h and b_1 are used instead of $h/\frac{1}{2}b$ and $b_1/\frac{1}{2}b$.

By equations (2–7) and (2–8), the power series for e_3 with respect to h begins:

$$e_3 = 1 - \left(\frac{b_1}{2}\right)^2 + \tfrac{1}{2}\frac{1+3\left(\frac{b_1}{2}\right)^2}{1-\left(\frac{b_1}{2}\right)^2}\left(\frac{h}{2}\right)^2 + \ldots \qquad (2\text{–}56)$$

At the position of the plate, $y = b_1/2 \pm 0$, by equations (2–10), (2–11) and (2–12)

$$y_3 = \pm\frac{hb_1}{2} + \ldots$$

and

$$z_4 = \mp\left[\sqrt{\left\{1-\left(\frac{b_1}{2}\right)^2\right\}} \mp \frac{hb_1}{4}\frac{1}{\sqrt{\left\{1-\left(\frac{b_1}{2}\right)^2\right\}}} + \ldots\right].$$

For $y \neq \frac{1}{2}b_1$, differentiate y_2 and y_3 with respect to h

$$\frac{\partial y_2}{\partial h} = \tfrac{1}{2}\left\{\frac{h}{2} \pm \frac{\left\{y_1 - \left(\frac{b_1}{2}\right)^2 + \left(\frac{h}{2}\right)^2\right\}\cdot\frac{h}{2} + \frac{hb_1^2}{4}}{\sqrt{\left[\left\{y_1 - \left(\frac{b_1}{2}\right)^2 + \left(\frac{h}{2}\right)^2\right\}^2 + \left(\frac{hb_1}{2}\right)^2\right]}}\right\}$$

$$\frac{\partial y_3}{\partial h} = \frac{\partial y_2}{\partial h} - \frac{h}{4} + \tfrac{1}{4}\frac{\frac{hb_1^2}{2} + 2\left(\frac{h}{2}\right)^3}{y_2 - \frac{1}{2}\left(\frac{h}{2}\right)^2} - \tfrac{1}{4}\left[\left(\frac{hb_1}{2}\right)^2 + \left(\frac{h}{2}\right)^4\right]\frac{\frac{\partial y_2}{\partial h} - \frac{h}{4}}{\left[y_2 - \frac{1}{2}\left(\frac{h}{2}\right)^2\right]^2}.$$

The right-hand sides contain a constant term only for $y = b_1/2$. This means that $y_3 - e_3$ and z_4 do not contain a term proportional to h. Hence by equations (2–25) and (2–38)

$$I = \frac{\pi}{2} + Ch^2 + \ldots$$

$$\varkappa = 1 - C_1h^2 + \ldots \qquad (2\text{–}57)$$

$$\frac{\Delta C_L c}{\bar{C}_L \bar{c}} = C_2h^2 + \ldots \text{ for } y \neq \frac{b_1}{2} \qquad (2\text{–}58)$$

$$\frac{\Delta C_L c}{\bar{C}_L \bar{c}} = \mp \frac{4}{\pi} \frac{\frac{b_1}{2}}{\sqrt{\left\{1 - \left(\frac{b_1}{2}\right)^2\right\}}} \frac{h}{2} + \ldots \text{ for } y = \frac{b_1}{2} \pm 0 . \quad .. \quad .. \quad (2\text{–}59)$$

Equations (2–57) to (2–59) show that small plates situated inboard of the tips have a negligible effect on the overall lift coefficient and change the load distribution only in the neighbourhood of the plate, as is to be expected.

For points on the plates, $|y_3| < hb_1/2$, and therefore by equations (2–15) and (2–16)

$$z_2 = \frac{z_1}{2} = z \frac{b_1}{2}$$

and by equation (2–14)

$$y_3 = \pm \frac{hb_1}{2} \sqrt{\left\{1 - \left(\frac{z}{h/2}\right)^2\right\}}$$

and

$$\begin{aligned} z_4 &= \sqrt{(e_2 - y_3)} \\ &= \sqrt{e_3} - \tfrac{1}{2} \frac{y_3}{\sqrt{e_3}} \\ &= \sqrt{e_3} \mp \frac{1}{\sqrt{e_3}} \frac{hb_1}{4} \sqrt{\left\{1 - \left(\frac{z}{h/2}\right)^2\right\}} \end{aligned}$$

$$\Delta z_4(z) = \frac{\frac{b_1}{2}}{\sqrt{\left\{1 - \left(\frac{b_1}{2}\right)^2\right\}}} h \sqrt{\left\{1 - \left(\frac{z}{h/2}\right)^2\right\}} . \quad .. \quad .. \quad .. \quad .. \quad (2\text{–}60)$$

For small plates the distribution of the side-force along the plate is elliptic and the local side-force coefficient is proportional to h/b. The latter can be obtained by combining equations (2–45) and (2–60), giving equation (2–53) which has been used above. Integration of equation (2–60) gives for the integral I_Y, equation (2–47)

$$I_Y = \frac{\frac{b_1}{2}}{\sqrt{\left\{1 - \left(\frac{b_1}{2}\right)^2\right\}}} \left(\frac{h}{2}\right)^2 \frac{\pi}{4}$$

and the coefficient of the side-force on the upper part of the plate is given by

$$\frac{\bar{C}_Y}{\bar{C}_L} = \frac{\frac{b_1}{2}}{\sqrt{\left\{1 - \left(\frac{b_1}{2}\right)^2\right\}}} \tfrac{1}{2} \left(\frac{h}{2}\right)^2 . \quad .. \quad .. \quad .. \quad .. \quad .. \quad (2\text{–}61)$$

With elliptic distribution of the side-force, the arm z_0, equation (2–50), is given by equation (2–51).

We consider now the case of end-plates, $b_1/2 = 1$. By equations (2–7) and (2–8)

$$e_3 = h + \ldots .$$

At the position of the plate, $y = 1 - 0$, by equations (2–10) and (2–11)

$$y_3 = -h + \ldots$$

and

$$\begin{aligned} z_4 &= \mp \sqrt{(e_3 - y_3)} \\ &= \mp \sqrt{(2h)} + \ldots \quad . \quad .. \quad .. \quad .. \quad .. \quad .. \quad .. \quad (2\text{–}62) \end{aligned}$$

For $y \neq 1$, by equations (2–9), (2–10) and (2–11)

$$y_3 = -(1 - y^2) + h^2(\ldots) .$$

Thus

$$z_4 = \mp \sqrt{(e_3 - y_3)}$$

$$|z_4| = \sqrt{(1 - y^2)} + \frac{\frac{h}{2}}{\sqrt{(1 - y}}$$

and by equation (2–25)

$$I = \frac{\pi}{2} + \frac{h}{2}\pi$$

$$= \frac{\pi}{2}(1 + h)$$

$$\varkappa = \frac{\pi/2}{I} = \frac{1}{1 + h}$$

$$= \frac{1}{1 + 2\frac{h}{b}} . \quad \ldots \quad \ldots \quad \ldots \quad \ldots \quad \ldots \quad \ldots \quad \ldots \quad (2\text{–}63)$$

Fig. 4 shows that this is a good approximation even if h/b is not very small. By equations (2–26), (2–62) and (2–63) the additional load at the plate is given by

$$\left(\frac{\Delta C_L c}{\bar{C}_L \bar{c}}\right)_{y=1} = \frac{4}{\pi}\frac{\sqrt{(2h)}}{1 + h}$$

$$= \frac{8}{\pi}\frac{\sqrt{(h/b)}}{1 + 2\frac{h}{b}} . \quad \ldots \quad \ldots \quad \ldots \quad \ldots \quad \ldots \quad \ldots \quad \ldots \quad (2\text{–}64)$$

The additional load away from the plate is given from equation (2–40), by

$$\frac{C_L c}{\bar{C}_L \bar{c}} - \frac{4}{\pi}\sqrt{\left\{1 - \left(\frac{y}{b/2}\right)^2\right\}} = \frac{4}{\pi}\frac{h/b}{1 + 2\frac{h}{b}}\frac{2\left(\frac{y}{b/2}\right)^2 - 1}{\sqrt{\left\{1 - \left(\frac{y}{b/2}\right)^2\right\}}} . \quad \ldots \quad \ldots \quad \ldots \quad \ldots \quad \ldots \quad (2\text{–}65)$$

3. *Plates on the Upper Surface of the Wing.*—3.1. *The Potential Function in the Trefftz-plane.* Of all wing-plate arrangements with varying ratios of the heights of the plates on the upper and lower surfaces of the wing, the extreme case of plates on the upper surface only is the simplest, having the smallest number of ' corners ', and we consider such an arrangement in this section.

To determine the load distribution over the wing, the potential function of the flow around the fixed wake contour is again calculated. The conformal transformations used are similar to those given by W. Mangler[1] for the general case of arbitrary ratio of the heights of the plates on the two surfaces. Let the plates be of height h.

As in the case where the plates are of equal height above and below the wing, the right half of the ζ-plane ($y > 0$) is transformed into the full ζ_1-plane by the transformation

$$\zeta_1 = -i\zeta^2 \quad \ldots \quad \ldots \quad \ldots \quad \ldots \quad \ldots \quad \ldots \quad \ldots \quad \ldots \quad (3\text{–}1)$$

(*see* Fig. 18).

The parabola, into which the plate is transformed, is again replaced by the arc of the circle through the points B_1 and C_1 and with its centre on the axis $z = 0$. The radius is

$$R = 2\left(\frac{b_1}{2}\right)^2 + \frac{h^2}{2}$$

and the centre is at

$$y_1 = -\left[\left(\frac{b_1}{2}\right)^2 + \frac{h^2}{2}\right].$$

The circle also intersects the y-axis at the point H_1:

$$\zeta_1 = -i\left[3\left(\frac{b_1}{2}\right)^2 + h^2\right].$$

In the next step, the circle and the y-axis are transformed into straight lines. This is achieved by a linear transformation which transforms the point H_1 into $y_2 \rightarrow -\infty$:

$$\zeta_2 = \frac{\zeta_1\left[1 + 3\left(\frac{b_1}{2}\right)^2 + h^2\right]}{-i\zeta_1 + 3\left(\frac{b_1}{2}\right)^2 + h^2}. \qquad \text{(3–2)}$$

The points A, B, C, D, E (*see* Fig. 18) are transformed into the points:

$$A_2 \quad : \zeta_2 = 0$$

$$\left.\begin{matrix} B_2 \\ D_2 \end{matrix}\right| \quad : \zeta_2 = i\frac{\left(\frac{b_1}{2}\right)^2\left[1 + 3\left(\frac{b_1}{2}\right)^2 + h^2\right]}{4\left(\frac{b_1}{2}\right)^2 + h^2}$$

$$C_2 \quad : \zeta_2 = -\frac{h}{b_1}\frac{\left[3\left(\frac{b_1}{2}\right)^2 + h^2\right]\left[1 + 3\left(\frac{b_1}{2}\right)^2 + h^2\right]}{4\left(\frac{b_1}{2}\right)^2 + h^2} + i\frac{\left(\frac{b_1}{2}\right)^2\left[1 + 3\left(\frac{b_1}{2}\right)^2 + h^2\right]}{4\left(\frac{b_1}{2}\right)^2 + h^2}$$

$$E_2 \quad : \zeta_2 = i.$$

The infinity in the ζ-plane, G, is transformed into

$$G_2 \quad : \zeta_2 = i\left[1 + 3\left(\frac{b_1}{2}\right)^2 + h^2\right].$$

The boundaries in the ζ_2-plane form a polygon, *see* Fig. 18; the outside of which can be transformed into the upper half of the ζ_3-plane by a Schwarz-Christoffel transformation:

$$\zeta_2 = C_1 + C_2\int_0^{\zeta_3}\frac{(t + ia_2)(t + ia_4)(t - i)}{\sqrt{\{(t + ia_1)(t + ia_3)\}t^2}}\,dt \qquad \text{(3–3)}$$

where $-ia_1$, $-ia_2$, $-ia_3$, $-ia_4$, correspond to B_3, C_3, D_3, E_3. The infinity in the ζ_2-plane, H_2, is transformed into $\zeta_3 = 0$, and the point G_2 into $\zeta_3 = i$.

Following the procedure used by W. Mangler, the integral in equation (3–3) can be written as an algebraic function:

$$\frac{\zeta_2}{i} = \lambda_1 + \left(\lambda_2 + i\lambda_3\frac{1}{\zeta_3}\right)\sqrt{\{-(ia_1 + \zeta_3)(ia_3 + \zeta_3)\}}. \qquad \text{(3–4)}$$

Differentiating equations (3–3) and (3–4) with respect to ζ_3 and comparing the coefficients of similar powers of ζ_3, we obtain the following equations:

$$C_2 = -\lambda_2 \quad .. \quad .. \quad .. \quad .. \quad .. \quad .. \quad .. \quad .. \quad (3\text{–}5)$$

$$\lambda_3 = \lambda_2 \frac{a_2 a_4}{a_1 a_3} \quad .. \quad .. \quad .. \quad .. \quad .. \quad .. \quad .. \quad .. \quad (3\text{–}6)$$

$$a_1 + a_3 = 2(a_2 + a_4 - 1) \quad .. \quad .. \quad .. \quad .. \quad .. \quad .. \quad (3\text{–}7)$$

$$a_1 + a_3 = 2\frac{a_1 a_3}{a_2 a_4}[a_2 + a_4 - a_2 a_4] \; . \quad .. \quad .. \quad .. \quad .. \quad .. \quad (3\text{–}8)$$

Introducing the abbreviations

$$A = 1 + \frac{a_1 + a_3}{2} \quad .. \quad .. \quad .. \quad .. \quad .. \quad .. \quad .. \quad (3\text{–}9)$$

$$B = a_1 a_3 \frac{a_1 + a_3 + 2}{a_1 + a_3 + 2a_1 a_3} \quad .. \quad .. \quad .. \quad .. \quad .. \quad .. \quad (3\text{–}10)$$

a_2 and a_4 can be calculated from a_1 and a_3:

$$a_2 = \tfrac{1}{2}\{A + \sqrt{(A^2 - 4B)}\} \; .. \quad .. \quad .. \quad .. \quad .. \quad .. \quad (3\text{–}11)$$

$$a_4 = \tfrac{1}{2}\{A - \sqrt{(A^2 - 4B)}\} \; . \quad .. \quad .. \quad .. \quad .. \quad .. \quad (3\text{–}12)$$

Equations for the unknown coefficients λ_1, λ_2, a_1, a_3 are obtained from the known positions of the points B_2, C_2, D_2, E_2, G_2 in the ζ_2-plane.

$\zeta_3 = -ia_1$ and $\zeta_3 = -ia_3$ correspond to

$$\frac{\zeta_2}{i} = \lambda_1 = \frac{\left(\frac{b_1}{2}\right)^2\left[1 + 3\left(\frac{b_1}{2}\right)^2 + h^2\right]}{4\left(\frac{b_1}{2}\right)^2 + h^2} \; . \quad .. \quad .. \quad .. \quad .. \quad (3\text{–}13)$$

$\zeta_3 = -ia_2$ corresponds to

$$\frac{\zeta_2}{i} = \lambda_1 + i\frac{h}{b_1}\frac{\left[3\left(\frac{b_1}{2}\right)^2 + h^2\right]\left[1 + 3\left(\frac{b_1}{2}\right)^2 + h^2\right]}{4\left(\frac{b_1}{2}\right)^2 + h^2}$$

$$= \lambda_1 - i\lambda_2\left(1 - \frac{a_4}{a_1 a_3}\right)\sqrt{\{(a_1 - a_2)(a_2 - a_3)\}} \; . \quad .. \quad .. \quad (3\text{–}14)$$

$\zeta_3 = -ia_4$ corresponds to

$$\frac{\zeta_2}{i} = 1 = \lambda_1 - \lambda_2\left(1 - \frac{a_2}{a_1 a_3}\right)\sqrt{\{(a_1 - a_4)(a_3 - a_4)\}} \; . \quad .. \quad .. \quad (3\text{–}15)$$

$\zeta_3 = i$ corresponds to

$$\frac{\zeta_2}{i} = 1 + 3\left(\frac{b_1}{2}\right)^2 + h^2 = \lambda_1 - \lambda_2\left(1 + \frac{a_2 a_4}{a_1 a_3}\right)\sqrt{\{(a_1 + 1)(a_3 + 1)\}} \; . \quad (3\text{–}16)$$

By equations (3–13), (3–14) and (3–16):

$$\frac{h}{b_1} = \frac{\left(1 - \frac{a_4}{a_1 a_3}\right)\sqrt{\{(a_1 - a_2)(a_2 - a_3)\}}}{\left(1 + \frac{a_2 a_4}{a_1 a_3}\right)\sqrt{\{(a_1 + 1)(a_3 + 1)\}}} \quad .. \quad .. \quad .. \quad .. \quad (3\text{–}17)$$

and by equations (3–13), (3–15) and (3–16):

$$\frac{1-\left(\frac{b_1}{2}\right)^2}{1+3\left(\frac{b_1}{2}\right)^2+h^2}=\frac{\left(1-\frac{a_2}{a_1a_3}\right)\sqrt{\{(a_1-a_4)(a_3-a_4)\}}}{\left(1+\frac{a_2a_4}{a_1a_3}\right)\sqrt{\{(a_1+1)(a_3+1)\}}} \quad \ldots\ldots\ldots\ldots \quad (3\text{–}18)$$

Using the abbreviation

$$D=\frac{\left(1-\frac{a_2}{a_1a_3}\right)\sqrt{\{(a_1-a_4)(a_3-a_4)\}}}{\left(1+\frac{a_2a_4}{a_1a_3}\right)\sqrt{\{(a_1+1)(a_3+1)\}}} \quad \ldots\ldots\ldots\ldots \quad (3\text{–}19)$$

we obtain

$$\left(\frac{b_1}{2}\right)^2=\frac{1-D}{1+3D+4D\left(\frac{h}{b_1}\right)^2} \quad \ldots\ldots\ldots\ldots \quad (3\text{–}20)$$

The constants a_1 and a_3 have to be chosen so that the required values of h and b_1 are obtained from equations (3–9) to (3–12), (3–17), (3–19) and (3–20). This has to be done numerically by varying a_1 and a_3.

The case of end-plates, $b_1/2 = 1{\cdot}0$, is simpler since $a_3 = a_4$. Then equations (3–7) and (3–8) give the relation

$$\frac{a_1a_3}{a_2}=1{\cdot}0 \quad \ldots\ldots\ldots\ldots \quad (3\text{–}21)$$

Instead of equations (3–11) and (3–12) we have

$$a_2=a_1\frac{2+a_1}{2a_1+1} \quad \ldots\ldots\ldots\ldots \quad (3\text{–}22)$$

$$a_3=\frac{2+a_1}{2a_1+1} \quad \ldots\ldots\ldots\ldots \quad (3\text{–}23)$$

and equation (3–17) is replaced by

$$\frac{h}{2}=\tfrac{1}{3}\left(\frac{a_1-1}{a_1+1}\right)^2\sqrt{\left\{\frac{(2+a_1)(2a_1+1)}{3a_1}\right\}} \quad \ldots\ldots\ldots \quad (3\text{–}24)$$

By equations (3–13) and (3–16)

$$\lambda_2=-\lambda_1\frac{3\left(\frac{b_1}{2}\right)^2+h^2}{\left(\frac{b_1}{2}\right)^2}\cdot\frac{1}{\left(1+\frac{a_2a_4}{a_1a_3}\right)\sqrt{\{(a_1+1)(a_3+1)\}}} \quad \ldots \quad (3\text{–}25)$$

The final relations between points on the y_3-axis and the wake contour are thus known. Points on the y_3-axis with $y_3 < -a_1$ or $y_3 > -a_3$ correspond to points on the wing:

$$y_2=\lambda_1\left[1\mp\frac{\left\{3\left(\frac{b_1}{2}\right)^2+h^2\right\}}{\left(\frac{b_1}{2}\right)^2}\frac{\left\{1+\frac{a_2a_4}{a_1a_3}\cdot\frac{1}{y_3}\right\}}{\left\{1+\frac{a_2a_4}{a_1a_3}\right\}}\frac{\sqrt{\{(a_1+y_3)(a_3+y_3)\}}}{\sqrt{\{(a_1+1)(a_3+1)\}}}\right] \quad (3\text{–}26)$$

and

$$y=\sqrt{y_1}=\sqrt{\left[\frac{y_2\left[3\left(\frac{b_1}{2}\right)^2+h^2\right]}{-y_2+1+3\left(\frac{b_1}{2}\right)^2+h^2}\right]} \quad \ldots\ldots\ldots \quad (3\text{–}27)$$

In equation (3–26) the negative sign holds for $y_3 < -a_1$, and the positive sign for $y_3 > -a_3$. Points with $-a_1 < y_3 < -a_3$ correspond to points on the plates:

$$z_2 = -\lambda_1 \frac{\left\{3\left(\frac{b_1}{2}\right)^2 + h^2\right\}}{\left(\frac{b_1}{2}\right)^2} \frac{\left\{1 + \frac{a_2 a_4}{a_1 a_3}\frac{1}{y_3}\right\}}{\left\{1 + \frac{a_2 a_4}{a_1 a_3}\right\}} \cdot \frac{\sqrt{\{(a_1 + y_3)(-y_3 - a_3)\}}}{\sqrt{\{(a_1 + 1)(a_3 + 1)\}}} \tag{3–28}$$

$$z = \tfrac{1}{2}\frac{z_1}{\frac{b_1}{2}} = \frac{1}{2\frac{b_1}{2}} \frac{z_2\left[1 + 3\left(\frac{b_1}{2}\right)^2 + h^2\right]\left[3\left(\frac{b_1}{2}\right)^2 + h^2\right]}{z_2^2 + \left[1 + 3\left(\frac{b_1}{2}\right)^2 + h^2 - \lambda_1\right]^2} \cdot \quad .. \quad .. \tag{3–29}$$

To determine the potential function in the ζ_3-plane, we will proceed to show that a parallel flow in the ζ-plane with the velocity $-v_{z\infty}$ parallel to the z-axis corresponds, in the ζ_3-plane, to the flow of a doublet at the point $\zeta_3 = i$, which corresponds to the point at infinity in the ζ-plane. The axis of the doublet is parallel to the y_3-axis.

For points in the neighbourhood of $\zeta_3 = i$

$$\frac{\zeta_2}{i} = 1 + 3\left(\frac{b_1}{2}\right)^2 + h^2 + C(\zeta_3 - i)^2 + \ldots \quad .. \quad .. \quad .. \tag{3–30}$$

since by equations (3–3) and (3–4)

$$\frac{d(\zeta_2/i)}{d\zeta_3} = 2C(\zeta_3 - i) + \ldots$$

with

$$C = \frac{\lambda_2}{2} \frac{(1 + a_2)(1 + a_4)}{\sqrt{\{(1 + a_1)(1 + a_3)\}}} \cdot \quad .. \quad .. \quad .. \quad .. \quad .. \tag{3–31}$$

By equations (3–1), (3–2) and (3–30) for $\zeta \to \infty$

$$\zeta = \sqrt{\left[\frac{\left[1 + 3\left(\frac{b_1}{2}\right)^2 + h^2\right]\left[3\left(\frac{b_1}{2}\right)^2 + h^2\right]}{C \cdot (\zeta_3 - i)^2}\right]}$$

$$= \sqrt{\left[\frac{\left[1 + 3\left(\frac{b_1}{2}\right)^2 + h^2\right]\left[3\left(\frac{b_1}{2}\right)^2 + h^2\right]}{-C}\right]} \frac{-1}{\frac{\zeta_3}{i} - 1} \cdot$$

Since the y_3-axis is a streamline in the doublet flow the complex potential function for the flow around the fixed wake contour is given by the potential of the doublet only

$$F_1(\zeta) = \phi_1(z,y) + i\psi_1(z,y)$$

$$= v_{z\infty} \frac{b}{2} \frac{\mu}{\frac{\zeta_3}{i} - 1} \quad .. \quad .. \quad .. \quad .. \quad .. \quad .. \tag{3–32}$$

where

$$\mu = \sqrt{\left[\frac{2\left[4 \cdot \left(\frac{b_1}{2}\right)^2 + h^2\right]\left[1 + \frac{a_2 a_4}{a_1 a_3}\right](a_1 + 1)(a_3 + 1)}{(a_2 + 1)(a_4 + 1)}\right]} \quad .. \tag{3–33}$$

and the total potential for the moving wake contour is

$$F(\zeta) = F_1(\zeta) + v_{z\infty}\zeta\frac{b}{2} \cdot$$

For points on the wing or the plates, the potential is

$$\phi(z,y) = v_{z\infty}\left[\frac{\mu}{y_3(z,y) - 1} + z\right]\frac{b}{2} \quad .. \quad .. \quad .. \quad .. \quad .. \quad (3\text{–}34)$$

where the function $y_3(z,y)$ is determined by equations (3–26) to (3–29).

3.2. *The Load Distribution on the Wing.*—From the known potential function, equation (3–34), we may obtain the load distribution along the wing by equation (2–22):

$$C_L(y) \cdot c(y) = 2\frac{v_{z\infty}}{V_0}\mu\left[\left(\frac{1}{y_3 - 1}\right)_{US} - \left(\frac{1}{y_3 - 1}\right)_{LS}\right]\cdot\frac{b}{2}$$

$$= 2\frac{v_{z\infty}}{V_0}\mu\Delta\left(\frac{1}{y_3 - 1}\right)_{Wing}\frac{b}{2}. \quad .. \quad .. \quad .. \quad .. \quad .. \quad (3\text{–}35)$$

The difference $\Delta\left(\frac{1}{y_3 - 1}\right)_{Wing}$ for corresponding points on the upper and lower surface of the wing has to be determined graphically.

The coefficient $\bar{C}_L$ of the overall lift is as in equation (2–24),

$$\bar{C}_L = A\frac{v_{z\infty}}{V_0}I \quad .. \quad .. \quad .. \quad .. \quad .. \quad .. \quad .. \quad (3\text{–}36)$$

with

$$I = \mu\int_0^1 \Delta\left(\frac{1}{y_3 - 1}\right)_{Wing} d\left(\frac{y}{b/2}\right). \quad .. \quad .. \quad .. \quad .. \quad .. \quad (3\text{–}37)$$

The method of determining the downwash is the same as in section 2.2 for the wing with plates of equal heights above and below the wing. For constant sectional lift slope, or with the assumption of equation (2–35), equations (2–37) and (2–38) hold, where $\varkappa$ is now calculated with the value of I given by equation (3–37). Some $\varkappa$ values are plotted in Fig. 19. The results show that with plates of the same total height, the plates on the upper surface have a somewhat larger effect than plates of equal height above and below the wing. There should be no difficulty in interpolating results for other wing-plate arrangements.

The spanwise load distribution is given by

$$\frac{C_L(y)}{\bar{C}_L}\frac{c(y)}{\bar{c}} = \frac{\mu}{I}\Delta\left(\frac{1}{y_3 - 1}\right)_{Wing}. \quad .. \quad .. \quad .. \quad .. \quad .. \quad .. \quad (3\text{–}38)$$

The additional load distribution is again determined by equation (2–40), where $C_Lc/\bar{C}_L\bar{c}$ is given by equation (3–38). Values of $\frac{C_Lc}{\bar{C}_L\bar{c}} - \frac{4}{\pi}\sqrt{\left\{1 - \left(\frac{y}{b/2}\right)^2\right\}}$ are plotted in Figs. 20 to 22 and tabulated in Table 3.

A comparison of the additional load distribution for plates of equal height above and below the wing and plates on the upper surface only, *see* Fig. 23, shows that the spanwise loading and in particular the values at the wing-plate junction are not much different in the two cases, so that it is possible to interpolate the values for plate arrangements with a ratio of the heights of the plates on the upper and lower surfaces of the wing different from the two extreme cases calculated. With plates on the outboard part of the span the additional load decreases in nearly the same way for the two cases, whilst with plates well inboard the additional load decreases more slowly with plates on the upper surface only.

3.3. *The Side-force on the Plates.*—The side-force on the plates is determined from the known difference of the potential function inside and outside the plate. By equations (2–43) and (3–34)

$$C_Y(z) \cdot c(y) = 2\frac{v_{z\infty}}{V_0}\mu\left[\left(\frac{1}{y_3-1}\right)_{\text{Inside}} - \left(\frac{1}{y_3-1}\right)_{\text{Outside}}\right]\frac{b}{2}$$

$$= 2\frac{v_{z\infty}}{V_0}\mu\Delta\left(\frac{1}{y_3-1}\right)_{\text{Plate}}\frac{b}{2} \quad \ldots\ldots\ldots\ldots\ldots\ldots \quad (3\text{–}39)$$

The local side-force coefficient referred to the total lift coefficient is

$$\frac{C_Y c}{\bar{C}_L \bar{c}} = \frac{\mu}{I}\Delta\left(\frac{1}{y_3-1}\right)_{\text{Plate}} \quad \ldots\ldots\ldots\ldots\ldots\ldots \quad (3\text{–}40)$$

Side-force distributions are plotted in Fig. 24. A comparison with Fig. 15 shows that the side-force coefficients on plates on the upper surface are about twice as large as on the upper part of plates above and below the wing of the same total height. This is to be expected as the area above the wing in the former case is twice that in the latter.

The coefficient of the total side-force on one plate is written as in equation (2–46)

$$\bar{C}_Y = A\frac{v_{z\infty}}{V_0}I_Y \quad \ldots\ldots\ldots\ldots\ldots\ldots \quad (3\text{–}41)$$

with

$$I_Y = \tfrac{1}{2}\mu\int_0^{h/\frac{1}{2}b}\Delta\left(\frac{1}{y_3-1}\right)_{\text{Plate}} d\left(\frac{z}{b/2}\right) \quad \ldots\ldots\ldots\ldots \quad (3\text{–}42)$$

$$\frac{\bar{C}_Y}{\bar{C}_L} = \frac{I_Y}{I} \quad \ldots\ldots\ldots\ldots\ldots\ldots \quad (3\text{–}43)$$

The ratio $\bar{C}_Y/\bar{C}_L$ is plotted in Fig. 25.

The moment M of the side-force with respect to the plate-wing junction has been determined from the side-force distribution in equation (3–40), *see* equation (2–49), and from this the arm

$$z_0\frac{b}{2} = \frac{M}{\bar{F}_Y}$$

has been calculated and plotted in Fig. 26. The approximation, equation (2–51), resulting from elliptic side-force distribution, is still of sufficient accuracy.

4. *Practical Example.*—This section gives a description of the actual calculation procedure. From the known plan-form of the wing*, the mean sectional lift slope $a = a_0 \cos\varphi$ is determined as well as the value of the downwash factor ω, as explained in Ref. 7. From the given position and height of the plates, values of the factor $\varkappa$ can be read from Fig. 4 for plates of the same height on the upper and lower surfaces of the wing and from Fig. 19 for plates on the upper surface only. The change in the overall lift slope due to the plates is determined from the relation

$$\frac{\Delta\bar{C}_L}{\alpha} = \frac{\bar{C}_{L0}}{\alpha}\left[\frac{1+\frac{\omega a}{\pi A}}{1+\varkappa\frac{\omega a}{\pi A}} - 1\right] \quad \ldots\ldots\ldots\ldots\ldots\ldots \quad (4\text{–}1)$$

$\bar{C}_{L0}/\alpha$ is the lift slope of the wing alone, which can be obtained either from a complete calculation according to Ref. 7, or from the approximate relation

$$\frac{\bar{C}_{L0}}{\alpha} = \frac{a}{1+\frac{\omega a}{\pi A}} \quad \ldots\ldots\ldots\ldots\ldots\ldots \quad (4\text{–}2)$$

* If the calculation is to be performed for a given subcritical Mach number, the plan-form of the analogous wing must be used (*see* Ref. 7).

The overall lift slope of the wing with plates is then given by

$$\frac{\bar{C}_L}{\alpha} = \frac{\bar{C}_{L0}}{\alpha} + \frac{\Delta\bar{C}_L}{\alpha}.$$

The additional spanwise load distribution is given by

$$\frac{\Delta C_L(y)}{\alpha}\frac{c(y)}{\bar{c}} = \frac{\bar{C}_L}{\alpha}\left[\frac{C_L c}{\bar{C}_L \bar{c}} - \frac{4}{\pi}\sqrt{\left\{1-\left(\frac{y}{b/2}\right)^2\right\}}\right] + \frac{\Delta\bar{C}_L}{\alpha}\frac{4}{\pi}\sqrt{\left\{1-\left(\frac{y}{b/2}\right)^2\right\}}. \qquad (4\text{–}3)$$

In most cases of practical importance $\Delta\bar{C}_L/\alpha$ is small compared with $\bar{C}_L/\alpha$, so the second term in equation (4–3) can be neglected.

Then from values of $\frac{C_L c}{\bar{C}_L \bar{c}} - \frac{4}{\pi}\sqrt{\left\{1-\left(\frac{y}{b/2}\right)^2\right\}}$ which are given in Figs. 5 to 10 and 20 to 23, and in Tables 2 and 3, and from $\bar{C}_L/\alpha$, we can calculate $\frac{\Delta C_L(y)}{\alpha}\frac{c(y)}{\bar{c}}$.

The distribution of the side-force along the plate is nearly elliptical; some distributions are plotted in Figs. 15 and 24. Total values of the side-force on the part of the plate on the upper surface of the wing are given in Figs. 16 and 25. The moment of the side-force with respect to the wing-plate junction may be obtained from Figs. 17 and 26.

As an illustration, we will calculate the load distribution of a swept wing with fences of varying spanwise position $b_1/2$ and various heights h. Let the wing be of aspect ratio 3, taper ratio 1 : 3, and let the sweep of the quarter-chord line be $\varphi_{c/4} = 50$ deg. The lift distribution of the wing alone, which has been calculated in Ref. 11 using the method of Ref. 7, is plotted in Fig. 27. Let the maximum height of the fences, h, be 0·2 and 0·4 times the local wing chord $c(y)$, i.e.,

$$\frac{h}{\bar{b}} = \left.\begin{matrix}0{\cdot}2\\0{\cdot}4\end{matrix}\right\} \times \frac{c/\bar{c}}{A} = \left.\begin{matrix}0{\cdot}2\\0{\cdot}4\end{matrix}\right\} \times \left[0{\cdot}5 - \tfrac{1}{3}\frac{b_1/2}{b/2}\right]$$

Let the fences be of the same height on the upper and lower surfaces of the wing.

From Fig. 4 we get $\varkappa = 0{\cdot}970$ for $b_1/2 = 0{\cdot}8b/2$ and $h/c = 0{\cdot}4$ (i.e., $h/b = 0{\cdot}093$). The values of the sectional lift slope a of the sheared wing, and of ω, for the wing alone are $a = 4{\cdot}4$, $\omega = 1{\cdot}04$. The overall lift slope of the wing alone is $\bar{C}_{L0}/\alpha = 2{\cdot}86$. With these values we may calculate the change of the total lift slope by equation (4–1)

$$\frac{\Delta\bar{C}_L}{\alpha} = 0{\cdot}03$$

$$\frac{\Delta\bar{C}_L}{\bar{C}_L} = 0{\cdot}01.$$

With smaller fences, or fences farther inboard on the wing, the value of $\Delta\bar{C}_L/\bar{C}_L$ is still smaller.

The additional lift, by equation (4–3), is

$$\frac{\Delta C_L(y)}{\bar{C}_L} = \frac{1}{c(y)/\bar{c}}\left\{\left[\frac{C_L c}{\bar{C}_L \bar{c}} - \frac{4}{\pi}\sqrt{\left\{1-\left(\frac{y}{b/2}\right)^2\right\}}\right] + \frac{\Delta\bar{C}_L}{\bar{C}_L}\frac{4}{\pi}\sqrt{\left\{1-\left(\frac{y}{b/2}\right)^2\right\}}\right\}. \qquad (4\text{–}4)$$

In the example chosen, the second term in equation (4–4) can be neglected. Values of $\frac{C_L c}{\bar{C}_L \bar{c}} - \frac{4}{\pi}\sqrt{\left\{1-\left(\frac{y}{b/2}\right)^2\right\}}$ for the given $\frac{b_1/2}{b/2}$ and h/b are interpolated between those given in Figs. 5 to 7 and Table 2. Adding the $\Delta C_L(y)/\bar{C}_L$ to those of the wing alone leads to the lift distributions plotted in Fig. 27.

LIST OF SYMBOLS

x, y, z		Rectangular system of co-ordinates, x in the wind direction, y spanwise, z positive downwards, *see* Fig. 2.
ζ	=	$z + iy$, complex co-ordinates in the Trefftz-plane.
ζ_ν	=	$z_\nu + iy_\nu$, complex co-ordinates in transformed Trefftz-planes, *see* Figs. 2 and 18.
c		Local wing chord.
$\bar{c}$		Mean chord of the wing.
b		Wing span.
h		Total height of the plates.
b_1		Spanwise distance of the plates.
A	=	$\frac{b}{\bar{c}}$, aspect ratio.
φ		Angle of sweep of mid-chord line.
α		Geometric incidence.
α_i		Induced angle of incidence.
α_e		Effective angle of incidence.
V_0		Velocity of the main flow.
$v_{z\,\infty}$		Downwash velocity in the Trefftz-plane.
ϕ		Potential function.
C_L		Local lift coefficient.
$\bar{C}_L$		Overall lift coefficient.
C_{L0}		Local lift coefficient of wing alone.
$\bar{C}_{L0}$		Overall lift coefficient of wing alone.
ΔC_L	=	$C_L - C_{L0}$
$\Delta \bar{C}_L$	=	$\bar{C}_L - \bar{C}_{L0}$
C_Y	=	$\frac{F_Y}{\frac{1}{2}\rho V_0^2 c}$, local side-force coefficient.
$\bar{C}_Y$	=	$\frac{\bar{F}_Y}{\frac{1}{2}\rho V_0^2 b\bar{c}}$, coefficient of the total side-force on the part of the plate on the upper surface of the wing.
M		Moment of the side-force on the upper part of the plate.
z_0	=	$\frac{M}{\bar{F}_Y \frac{b}{2}}$, moment arm.
a	=	$\frac{C_L}{\alpha_e}$, sectional lift slope, *see* Ref. 7.
a_0		Lift slope of the two-dimensional aerofoil.
ω	=	$\frac{\alpha_i}{\frac{1}{2}v_{z\,\infty}/V_0}$, downwash factor, *see* Ref. 7.
$\varkappa$	=	$\frac{\pi}{2I}$
I		*See* equations (2–24), (2–25) and (3–37).
I_Y		*See* equations (2–46), (2–47) and (3–42).
μ		Strength of doublet in ζ_3-plane, *see* equations (3–32) and (3–33).

REFERENCES

No.	*Author*	*Title, etc.*
1	W. Mangler :	Lift distribution around aerofoils with endplates. *L.F.F.* Vol. 16, p. 219. 1939. A.R.C. 8237. December, 1944. RTP Trans No. 2338.
2	D. Küchemann	Types of flow on swept wings with special reference to free boundaries and vortex sheets. *J.R.Ae.Soc.* Vol. 57, p. 683. November, 1953.
3	J. Weber and J. A. Lawford	The reflection effect of fences at low speeds. A.R.C. 17,060. May, 1954.
4	A. Betz	*Konforme Abbildung.* p. 249. Springer-Verlag, Berlin, 1948.
5	J. Weissinger	Die Auftriebsverteilung von Tragflügeln mit Tiefensprung. *Ingenieur-Archiv.* Vol. 20, p. 166. 1952.
6	J. Weissinger	Über die Einschaltung zusätzlicher Punkte beim Verfahren von Multhopp. *Ingenieur-Archiv.* Vol. 20, p. 163. 1952.
7	D. Küchemann	A simple method of calculating the span and chordwise loading on straight and swept wings of any given aspect ratio at subsonic speeds. R. & M. 2935. August, 1952.
8	V. M. Falkner and Sir Charles Darwin	The design of minimum drag tip fins. R. & M. 2279. March, 1945.
9	D. Küchemann and D. J. Kettle ..	The effect of endplates on swept wings. C.P. 104. June, 1951.
10	J. Weber	Theoretical load distribution on a wing with a cylindrical body at one end. R. & M. 2889. June, 1952.
11	J. A. Bagley	Some examples of the calculated effect of angle of sweep and taper on the lift distribution of a wing. R.A.E. Tech. Note Aero. 2202. November, 1952.
12	D. E. Hartley	Theoretical load distributions on wings with tip-tanks. C.P. 147. June, 1952.

APPENDIX I

The Load Distribution on Wings with a Discontinuity in Chord, Sectional Lift Slope or Geometric Incidence

The local lift is determined by the equation

$$\gamma(\eta) = \frac{C_L(\eta) \cdot c(\eta)}{2b} = \frac{a(\eta) \cdot c(\eta)}{2b} \cdot (\alpha(\eta) - \omega\alpha_{i\,0}(\eta)) \quad \ldots \quad \text{(A–1)}$$

where $\eta = y/\frac{1}{2}b$, b is the wing span, $a(\eta)$ is the sectional lift slope, $c(\eta)$ is the local chord, and $\alpha(\eta)$ is the geometric incidence. The induced incidence, $\alpha_i = \omega\alpha_{i0}(\eta)$, is a function of the trailing vortex sheet

$$\alpha_{i\,0}(\eta) = \frac{1}{2\pi}\int_{-1}^{+1} \frac{d\gamma}{d\eta'} \frac{d\eta'}{\eta - \eta'} \cdot \quad \ldots \quad \text{(A–2)}$$

$\omega/2$ is the ratio between the induced downwash at the wing and that far downstream in the wake; $\omega = 1$ for wings of large aspect ratio and $\omega \to 2$ as $A \to 0$ (*see* Ref. 7).

The spanwise load distribution $\gamma(\eta)$ is always a continuous function, but the induced incidence $\alpha_i(\eta)$ can be discontinuous. Such a discontinuous α_i exists for a discontinuity in the geometric incidence $\alpha(\eta)$ or the chord $c(\eta)$ or the sectional lift slope $a(\eta)$.

When the incidence distribution $\alpha(\eta)$ has a discontinuity, the induced incidence has the same discontinuity. For this case H. Multhopp has solved equation (A–1) by calculating $\gamma(\eta)$ as the sum of two terms

$$\gamma(\eta) = \gamma_I(\eta) + \gamma^*(\eta) \cdot \quad \ldots \quad \text{(A–3)}$$

The first term, $\gamma_I(\eta)$, depends only on the amount and the position of the discontinuity. The second term, $\gamma^*(\eta)$, belongs to a continuous $\alpha(\eta)$ distribution and can be calculated by the usual methods.

With a discontinuity in the chord the method has to be altered since the amount of the discontinuity of α_i is not known beforehand. The distribution γ_I which takes account of the discontinuity, depends on the unknown value of the total γ at the position of the discontinuity. An extension of Multhopp's method for calculating the load distribution over a wing which has a discontinuity in the chord has been given by J. Weissinger[5].

The Multhopp-Weissinger method can be extended to swept wings and to wings of small aspect ratio by using a method similar to that used by D. Küchemann for ordinary swept wings, *i.e.*, by introducing a sectional lift slope $a(\eta)$ which depends on sweep and varies along the span, and by using the downwash factor ω which depends on the aspect ratio of the wing. In the following, the calculation procedure will be written down for the general case of a discontinuity in incidence, chord and lift slope. The latter may not exist in practice but only in approximate representations. To simplify matters for the reader, we repeat here the work of Weissinger.

Since the position of the discontinuity will not in general coincide with one of the fixed pivotal points of Multhopp's calculation procedure, it is advisable to extend this calculation so as to allow the calculation of the load distribution at one further arbitrary point along the span. Multhopp approximates the γ-function by the interpolation function

$$\bar{\gamma}(\vartheta) = \frac{2}{m+1} \sum_{n=1}^{m} \gamma_n \sum_{\mu=1}^{m} \sin\mu\vartheta_n \sin\mu\vartheta \quad \ldots \quad \text{(A–4)}$$

where

$$\eta = \cos\vartheta$$

$$\gamma_n = \gamma(\vartheta_n) \text{ with } \vartheta_n = \frac{n\pi}{m+1} \cdot$$

Let

$$\eta_s = \cos \vartheta_s$$

be the position of the arbitrary point. The function

$$\gamma(\vartheta) = \bar{\gamma}(\vartheta) + \frac{\gamma(\vartheta_s) - \bar{\gamma}(\vartheta_s)}{\sin (m+1)\vartheta_s} \sin (m+1)$$

has the values

$$\gamma(\vartheta_\nu) = \bar{\gamma}(\vartheta_\nu) = \gamma_\nu$$
$$\gamma(\vartheta_s) = \qquad\quad \gamma_s .$$

Now

$$\alpha_{i\,0}(\vartheta) = \frac{1}{2\pi} \int_0^\pi \frac{d\gamma}{d\vartheta'} \frac{d\vartheta'}{\cos \vartheta' - \cos \vartheta}$$

$$= \frac{1}{2\pi} \int_0^\pi \frac{d\bar{\gamma}}{d\vartheta'} \frac{d\vartheta'}{\cos \vartheta' - \cos \vartheta} + \frac{\gamma_s - \bar{\gamma}(\vartheta_s)}{\sin (m+1)\vartheta_s} \cdot \frac{(m+1) \sin (m+1)\vartheta}{2 \sin \vartheta} .$$

This gives

$$\alpha_{i\,0}(\vartheta_\nu) = b_{\nu\nu}\gamma_\nu - \sum_{n=1}^{m}{}' b_{\nu n}\gamma_n$$

where $b_{\nu\nu}$ and $b_{\nu n}$ are the coefficients given by Multhopp. This means that the calculation of γ at the positions η_ν is not affected by the additional point η_s.

The induced incidence at η_s is

$$\alpha_{i\,0}(\vartheta_s) = \frac{1}{2\pi} \int_0^\pi \frac{d\bar{\gamma}}{d\vartheta'} \frac{d\vartheta'}{\cos \vartheta' - \cos \vartheta_s} + [\gamma_s - \bar{\gamma}(\vartheta_s)] \frac{m+1}{2 \sin \vartheta_s} .$$

This is equal to

$$\alpha_{i\,0}(\vartheta_s) = b_{ss}\gamma_s - \sum_{n=1}^{m} b_{sn}\gamma_n \qquad \text{(A–5)}$$

where

$$b_{ss} = \frac{m+1}{2 \sin \vartheta_s} \qquad \text{(A–6)}$$

$$b_{sn} = \frac{1}{(m+1) \sin \vartheta_s} \sum_{\mu=1}^{m} (m+1-\mu) \sin \mu\vartheta_n \sin \mu\vartheta_s$$

$$= \frac{a_{sn} \sin \vartheta_n}{(m+1)(\cos \vartheta_s - \cos \vartheta_n)^2} \qquad \text{(A–7)}$$

$$a_{sn} = \begin{cases} \sin^2 \dfrac{(m+1)\vartheta_s}{2} & n \text{ even} \\ \cos^2 \dfrac{(m+1)\vartheta_s}{2} & n \text{ odd} . \end{cases} \qquad \text{(A–8)}$$

The value γ_s can be determined from the equation

$$\gamma_s = \frac{a(\eta_s)\, c(\eta_s)}{2b} [\alpha(\eta_s) - \omega\alpha_{i\,0}(\eta_s)] \qquad \text{(A–9)}$$

by inserting equation (A–5). This is a better approximation for γ_s than the value $\bar{\gamma}(\vartheta_s)$ obtained from equation (A–4), since it is based on the values $a(\eta_s)$, $c(\eta_s)$, $\alpha(\eta_s)$. In the case of symmetrical load distributions

$$\alpha_{i\,0}(\vartheta_s) = b_{ss}\gamma_{ss} - \sum_{n=1}^{\frac{m+1}{2}} B_{sn}\gamma_n \qquad \text{(A–10)}$$

with

$$B_{sn} = b_{sn} + b_{s,\,m+1-n} \qquad \text{(A–11)}$$

$$B_{s\,\frac{m+1}{2}} = b_{s\,\frac{m+1}{2}} \qquad \text{(A–12)}$$

It is now assumed that, at the spanwise positions $\pm\,\eta_s$, the incidence, the chord and the sectional lift slope have discontinuities, but that they are continuous everywhere else.

Defining

$$\sigma = \alpha(\eta_s + 0) - \alpha(\eta_s - 0) \qquad \text{(A–13)}$$

and

$$\tau = \frac{2b}{a(\eta_s - 0)c(\eta_s - 0)} - \frac{2b}{a(\eta_s + 0)c(\eta_s + 0)}$$

$$= 2b\,\frac{a(\eta_s + 0)c(\eta_s + 0) - a(\eta_s - 0)c(\eta_s - 0)}{a(\eta_s + 0)c(\eta_s + 0)\;a(\eta_s - 0)c(\eta_s - 0)}\,. \qquad \text{(A–14)}$$

Since the load distribution must be continuous everywhere, the following equation must hold

$$\gamma(\eta_s + 0) = \gamma(\eta_s - 0) = \gamma_s$$

$$= \frac{a(\eta_s + 0)c(\eta_s + 0)}{2b}\,[\alpha(\eta_s + 0) - \omega\alpha_{i\,0}(\eta_s + 0)]$$

$$= \frac{a(\eta_s - 0)c(\eta_s - 0)}{2b}\,[\alpha(\eta_s - 0) - \omega\alpha_{i\,0}(\eta_s - 0)]\,.$$

This demands a discontinuity of the induced incidence

$$\omega[\alpha_{i\,0}(\eta_s + 0) - \alpha_{i\,0}(\eta_s - 0)] = \tau\gamma_s + \sigma\,.$$

Multhopp has shown that the load distribution

$$\gamma_I(\eta) = \frac{\tau\gamma_s + \sigma}{\omega}\,F(\eta) \qquad \text{(A–15)}$$

with

$$F(\eta) = \frac{2}{\pi}\left[(\cos\vartheta - \cos\vartheta_s)\,\ln\frac{\sin\frac{1}{2}(\vartheta + \vartheta_s)}{\sin\frac{1}{2}|\vartheta - \vartheta_s|} + (\cos\vartheta + \cos\vartheta_s)\,\ln\frac{\cos\frac{1}{2}(\vartheta + \vartheta_s)}{\cos\frac{1}{2}(\vartheta - \vartheta_s)} + 2\vartheta_s\sin\vartheta\right]$$

$$\vartheta = \cos^{-1}\eta\,, \qquad \text{(A–16)}$$

produces the required discontinuity in the induced incidence

$$\omega\alpha_{i\,0\,I} = \begin{cases} 0 & \text{for } 0 \leqslant \eta < \eta_s \\ \tau\gamma_s + \sigma & \text{for } \eta_s < \eta \leqslant 1 \end{cases} \qquad \text{(A–17)}$$

$\gamma(\eta)$ can again be determined as the sum of $\gamma_I(\eta)$ and a further term $\gamma^*(\eta)$, equation (A–3), where $\gamma^*(\eta)$ has to satisfy the equation

$$\gamma^*(\eta) = \frac{a(\eta)\,.\,c(\eta)}{2b}\left[\alpha(\eta) - \omega\alpha_{i\,0\,I} - \frac{\gamma_I(\eta)\,.\,2b}{a(\eta)\,.\,c(\eta)} - \omega\alpha^*_{i\,0}(\eta)\right]. \qquad \text{(A–18)}$$

Since the remaining induced incidence $\omega\alpha^*_{i\,0}(\eta)$ is a continuous function, it can be approximately represented in the usual way by a sum of the load coefficients at certain points

$$\alpha^*_{i\,0\nu} = b_{\nu\nu}\gamma^*_\nu - \sum_{n=1}^{\frac{m+1}{2}}{}' B_{\nu n}\gamma^*_n \quad .. \quad .. \quad .. \quad .. \quad .. \quad .. \quad .. \quad \text{(A–19)}$$

$$\alpha^*_{i\,0\,s} = b_{ss}\gamma^*_s - \sum_{n=1}^{\frac{m+1}{2}} B_{sn}\gamma^*_n \,. \quad .. \quad .. \quad .. \quad .. \quad .. \quad .. \quad .. \quad \text{(A–20)}$$

It follows from

$$\gamma_s = \frac{\tau\gamma_s + \sigma}{\omega} F_s + \gamma^*_s$$

for $\omega - \tau F_s \neq 0$

that

$$\gamma_s = \frac{\omega\gamma^*_s + \sigma F_s}{\omega - \tau F_s} \quad .. \quad .. \quad .. \quad .. \quad .. \quad .. \quad .. \quad .. \quad \text{(A–21)}$$

hence

$$\gamma_I(\eta) = \frac{\sigma + \tau\gamma^*_s}{\omega - \tau F_s} F(\eta) \,. \quad .. \quad .. \quad .. \quad .. \quad .. \quad .. \quad .. \quad \text{(A–22)}$$

Inserting equations (A–17), (A–19), (A–20) and (A–22) into (A–18) we obtain, as the final equations for γ^*_ν and γ^*_s:

$$\gamma^*_\nu\left[b_{\nu\nu} + \frac{2b}{\omega a_\nu c_\nu}\right] = \frac{\alpha_\nu}{\omega} + \sum_{n=1}^{\frac{m+1}{2}}{}' B_{\nu n}\gamma^*_n - A_\nu \quad .. \quad .. \quad .. \quad .. \quad .. \quad .. \quad .. \quad \text{(A–23)}$$

where

$$A_\nu = \frac{\sigma + \tau\gamma^*_s}{\omega - \tau F_s} F_\nu \frac{2b}{\omega a_\nu c_\nu} \qquad \text{for} \quad 0 \leqslant \eta < \eta_s$$

$$A_\nu = \frac{\sigma + \tau\gamma^*_s}{\omega - \tau F_s}\left[1 + F_\nu \frac{2b}{\omega a_\nu c_\nu}\right] \quad \text{for} \quad \eta_s < \eta \leqslant 1$$

$$\gamma^*_s\left[b_{ss} + \frac{\omega}{\omega - \tau F_s}\frac{2b}{\omega a(\eta_s - 0)c(\eta_s - 0)}\right]$$

$$= \frac{\alpha(\eta_s - 0)}{\omega} + \sum_{n=1}^{\frac{m+1}{2}} B_{sn}\gamma^*_n - \frac{\sigma}{\omega - \tau F_s} F_s \frac{2b}{\omega a(\eta_s - 0)c(\eta_s - 0)} \,. \quad .. \quad \text{(A–24)}$$

The equations (A–23) and (A–24) are solved by an iteration process. When $\tau \neq 0$, a first approximation for $\gamma^{*(0)}(\eta)$ is determined by assuming $\gamma^{(0)}(\eta)$ and in particular $\gamma_s^{(0)}$ and calculating $\gamma_I^{(0)}(\eta)$ by equation (A–15) and $\gamma^{*,0)}(\eta)$ by equation (A–3). Having calculated $\gamma^*(\eta)$ and in particular γ^*_s, γ_s is calculated by equation (A–21), $\gamma_I(\eta)$ by equation (A–15) and $\gamma(\eta)$ by equation (A–3).

TABLE 1

Position of Certain Points in the Various ζ-planes, for the Case of Plates of Equal Height Above and Below the Wing

	$\zeta =$	$\zeta_1 =$	$\zeta_2 =$	$\zeta_3 =$	$\zeta_4 =$
A	0	0	$-i\left(\frac{b_1}{2}\right)^2$	$-i\left[\left(\frac{b_1}{2}\right)^2+\frac{1}{2}\left(\frac{h}{2}\right)^2+\frac{\left(\frac{b_1 h}{2}\right)^2+\left(\frac{h}{2}\right)^4}{b_1^2+2\left(\frac{h}{2}\right)^2}\right]$	$-\sqrt{\left[e_3+\left(\frac{b_1}{2}\right)^2+\frac{1}{2}\left(\frac{h}{2}\right)^2+\frac{\left(\frac{b_1 h}{2}\right)^2+\left(\frac{h}{2}\right)^4}{b_1^2+2\left(\frac{h}{2}\right)^2}\right]}$
B	$i\frac{b_1}{2}$	$i\left(\frac{b_1}{2}\right)^2$	$-i\cdot\frac{1}{2}\left[\sqrt{\left\{\left(\frac{hb_1}{2}\right)^2+\left(\frac{h}{2}\right)^4\right\}}-\left(\frac{h}{2}\right)^2\right]$	$-i\sqrt{\left\{\left(\frac{hb_1}{2}\right)^2+\left(\frac{h}{2}\right)^4\right\}}$	$-\sqrt{\left[e_3+\sqrt{\left\{\left(\frac{hb_1}{2}\right)^2+\left(\frac{h}{2}\right)^4\right\}}\right]}$
C	$-\frac{h}{2}+i\frac{b_1}{2}$	$-\frac{hb_1}{2}$ $+i\left[\left(\frac{b_1}{2}\right)^2-\left(\frac{h}{2}\right)^2\right]$	$-\frac{hb_1}{4}$	$-i\left(\frac{h}{2}\right)^2$	$-\sqrt{\left\{e_3+\left(\frac{h}{2}\right)^2\right\}}$
D	$i\frac{b_1}{2}$	$i\left(\frac{b_1}{2}\right)^2$	$i\cdot\frac{1}{2}\left[\sqrt{\left\{\left(\frac{hb_1}{2}\right)^2+\left(\frac{h}{2}\right)^4\right\}}+\left(\frac{h}{2}\right)^2\right]$	$i\sqrt{\left\{\left(\frac{hb_1}{2}\right)^2+\left(\frac{h}{2}\right)^4\right\}}$	$-\sqrt{\left[e_3-\sqrt{\left\{\left(\frac{hb_1}{2}\right)^2+\left(\frac{h}{2}\right)^4\right\}}\right]}$
E	i	i	$ie_2=i\cdot\frac{1}{2}\left\{1-\left(\frac{b_1}{2}\right)^2+\left(\frac{h}{2}\right)^2+\sqrt{\left[\left\{1-\left(\frac{b_1}{2}\right)^2+\left(\frac{h}{2}\right)^2\right\}^2+\left(\frac{hb_1}{2}\right)^2\right]}\right\}$	$ie_3=i\left[e_2-\frac{1}{2}\left(\frac{h}{2}\right)^2+\frac{1}{4}\frac{\left(\frac{b_1 h}{2}\right)^2+\left(\frac{h}{2}\right)^4}{e_2-\frac{1}{2}\left(\frac{h}{2}\right)^2}\right]$	0
Any point on the wing	iy	$iy_1=iy^2$	$iy_2=i\cdot\frac{1}{2}\left\{y_1-\left(\frac{b_1}{2}\right)^2+\left(\frac{h}{2}\right)^2\pm\sqrt{\left[\left\{y_1-\left(\frac{b_1}{2}\right)^2+\left(\frac{h}{2}\right)^2\right\}^2+\left(\frac{hb_1}{2}\right)^2\right]}\right\}$ $0\leqslant y<\frac{b_1}{2}:y_2<0$ $\frac{b_1}{2}<y\leqslant 1:y_2>0$	$iy_3=i\left[y_2-\frac{1}{2}\left(\frac{h}{2}\right)^2+\frac{1}{4}\frac{\left(\frac{b_1 h}{2}\right)^2+\left(\frac{h}{2}\right)^4}{y_2-\frac{1}{2}\left(\frac{h}{2}\right)^2}\right]$	$\mp\sqrt{(e_3-y_2)}$

TABLE 2

Values of $\frac{C_L(y)}{\bar{C}_L}\frac{c(y)}{\bar{c}} - \frac{4}{\pi}\sqrt{\left\{1-\left(\frac{y}{b/2}\right)^2\right\}}$ *for plates of equal height above and below the wing**

$\frac{y}{b/2}$	$b_1/b = 0{\cdot}2$				$b_1/b = 0{\cdot}4$				$b_1/b = 0{\cdot}6$			
	$\frac{h}{b}=0{\cdot}05$	0·1	0·2	0·3	0·05	0·1	0·2	0·3	0·05	0·1	0·2	0·3
0	0·002	0·012	0·044	0·091	0·002	0·009	0·038	0·078	0·001	0·005	0·020	0·041
0·1	0·004	0·015	0·049	0·096	0·002	0·011	0·041	0·082	0·001	0·006	0·022	0·045
0·15	0·006	0·019	0·055	0·104								
0·2	0·014	0·029	0·067	0·115	0·004	0·014	0·051	0·096	0·002	0·008	0·028	0·055
	−0·013	−0·024	−0·047	−0·073								
0·25	−0·005	−0·014	−0·036	−0·061								
0·3	−0·003	−0·009	−0·027	−0·050	0·007	0·024	0·071	0·123	0·003	0·011	0·039	0·073
0·35					0·013	0·034	0·089	0·141				
0·4	−0·001	−0·005	−0·017	−0·035	0·028	0·056	0·113	0·168	0·005	0·018	0·059	0·104
					−0·028	−0·055	−0·110	−0·164				
0·45					−0·012	−0·033	−0·086	−0·137				
0·50	−0·001	−0·003	−0·012	−0·025	−0·007	−0·023	−0·067	−0·117	0·011	0·035	0·097	0·154
0·55									0·021	0·052	0·126	0·188
0·6	0	−0·002	−0·009	−0·019	−0·004	−0·013	−0·044	−0·086	0·047	0·091	0·169	0·233
									−0·048	−0·097	−0·191	−0·276
0·65									−0·023	−0·058	−0·148	−0·231
0·7	0	−0·002	−0·006	−0·015	−0·002	−0·009	−0·031	−0·063	−0·013	−0·041	−0·117	−0·195
0·75												
0·8	0	−0·001	−0·005	−0·011	−0·001	−0·006	−0·022	−0·046	−0·007	−0·022	−0·074	−0·135
0·85												
0·90	0	−0·001	−0·003	−0·007	−0·001	−0·004	−0·014	−0·030	−0·003	−0·013	−0·044	−0·084
0·95	0	−0·001	−0·002	−0·004	0	−0·003	−0·010	−0·020	−0·002	−0·008	−0·030	−0·057
1·0	0	0	0	0	0	0	0	0	0	0	0	0

$\frac{y}{b/2}$	$b_1/b = 0{\cdot}8$				$b_1/b = 0{\cdot}9$				$b_1/b = 1{\cdot}0$			
	$\frac{h}{b}=0{\cdot}05$	0·1	0·2	0·3	0·05	0·1	0·2	0·3	0·05	0·1	0·2	0·3
0	−0·003	−0·009	−0·026	−0·040	−0·012	−0·031	−0·075	−0·107	−0·055	−0·098	−0·158	−0·197
0·1	−0·003	−0·008	−0·024	−0·037	−0·011	−0·030	−0·073	−0·103	−0·054	−0·096	−0·156	−0·193
0·15												
0·2	−0·002	−0·006	−0·018	−0·028	−0·010	−0·028	−0·066	−0·094	−0·051	−0·091	−0·146	−0·181
0·25												
0·3	−0·001	−0·003	−0·008	−0·011	−0·009	−0·023	−0·055	−0·079	−0·047	−0·083	−0·131	−0·161
0·35												
0·4	0·001	0·002	0·007	0·014	−0·007	−0·017	−0·037	−0·050	−0·040	−0·070	−0·109	−0·132
0·45												
0·50	0·003	0·010	0·031	0·053	−0·003	−0·007	−0·011	−0·010	−0·030	−0·052	−0·077	−0·090
0·55												
0·6	0·008	0·024	0·071	0·112	0·003	0·009	0·027	0·045	−0·017	−0·027	−0·033	−0·032
0·65												
0·7	0·019	0·057	0·141	0·200	0·012	0·034	0·087	0·130	0·002	0·010	0·030	0·048
0·75	0·035	0·087	0·193	0·264								
0·8	0·081	0·154	0·269	0·337	0·032	0·086	0·187	0·249	0·031	0·067	0·126	0·166
	−0·084	−0·163	−0·289	−0·377								
0·85	−0·037	−0·095	−0·211	−0·296	0·063	0·138	0·265	0·326				
0·90	−0·021	−0·060	−0·151	−0·223	0·129	0·239	0·377	0·449	0·088	0·179	0·291	0·353
					−0·117	−0·209	−0·312	−0·368				
0·95	−0·012	−0·034	−0·089	−0·146	−0·051	−0·103	−0·189	−0·236	0·160	0·295	0·434	0·504
1·0	0	0	0	0	0	0	0	0	0·517	0·675	0·827	0·899

* The values for $h/b = 0{\cdot}05$ are obtained by graphical interpolation.

TABLE 3

Values of $\frac{C_L(y)}{\bar{C}_L}\,\frac{c(y)}{\bar{c}} - \frac{4}{\pi}\sqrt{\left\{1-\left(\frac{y}{b/2}\right)^2\right\}}$ *for plates on upper surface of wing*

$\frac{y}{b/2}$	$b_1/b=0\cdot2$	$b_1/b=0\cdot4$		$b_1/b=0\cdot6$		$b_1/b=0\cdot8$		$b_1/b=1\cdot0$		
	$\frac{h}{b}=0\cdot1$	$0\cdot1$	$0\cdot2$	$0\cdot1$	$0\cdot2$	$0\cdot1$	$0\cdot2$	$0\cdot05$	$0\cdot1$	$0\cdot2$
0	0·023	0·017	0·071	0·013	0·040	−0·014	−0·028	−0·056	−0·101	−0·156
0·1	0·026	0·018	0·076	0·013	0·041	−0·013	−0·027	−0·055	−0·099	−0·153
0·15	0·029									
0·2	0·033 / −0·026	0·020	0·084	0·014	0·045	−0·011	−0·021	−0·053	−0·093	−0·142
0·25	−0·020									
0·3	−0·017	0·030	0·098	0·018	0·056	−0·008	−0·009	−0·048	−0·084	−0·125
0·35		0·041	0·106							
0·4	−0·011	0·060 / −0·051	0·118 / −0·113	0·029	0·076	−0·001	0·010	−0·042	−0·070	−0·101
0·45		−0·039	−0·102							
0·50	−0·007	−0·030	−0·092	0·051	0·104	0·013	0·041	−0·032	−0·051	−0·068
0·55				0·067	0·122					
0·6	−0·004	−0·020	−0·073	0·086 / −0·098	0·148 / −0·194	0·040	0·084	−0·018	−0·024	−0·022
0·65				−0·078	−0·168					
0·7	−0·003	−0·013	−0·057	−0·062	−0·145	0·082	0·140	0·004	0·014	0·041
0·75						0·110	0·177			
0·8	−0·002	−0·009	−0·042	−0·038	−0·104	0·147 / −0·150	0·222 / −0·258	0·039	0·077	0·128
0·85						−0·112	−0·210			
0·9	−0·001	−0·006	−0·027	−0·023	−0·062	−0·081	−0·163	0·109	0·190	0·270
0·95			−0·018	−0·016	−0·040	−0·055	−0·110	0·177	0·290	0·390
1·0	0	0	0	0	0	0	0	0·450	0·575	0·700

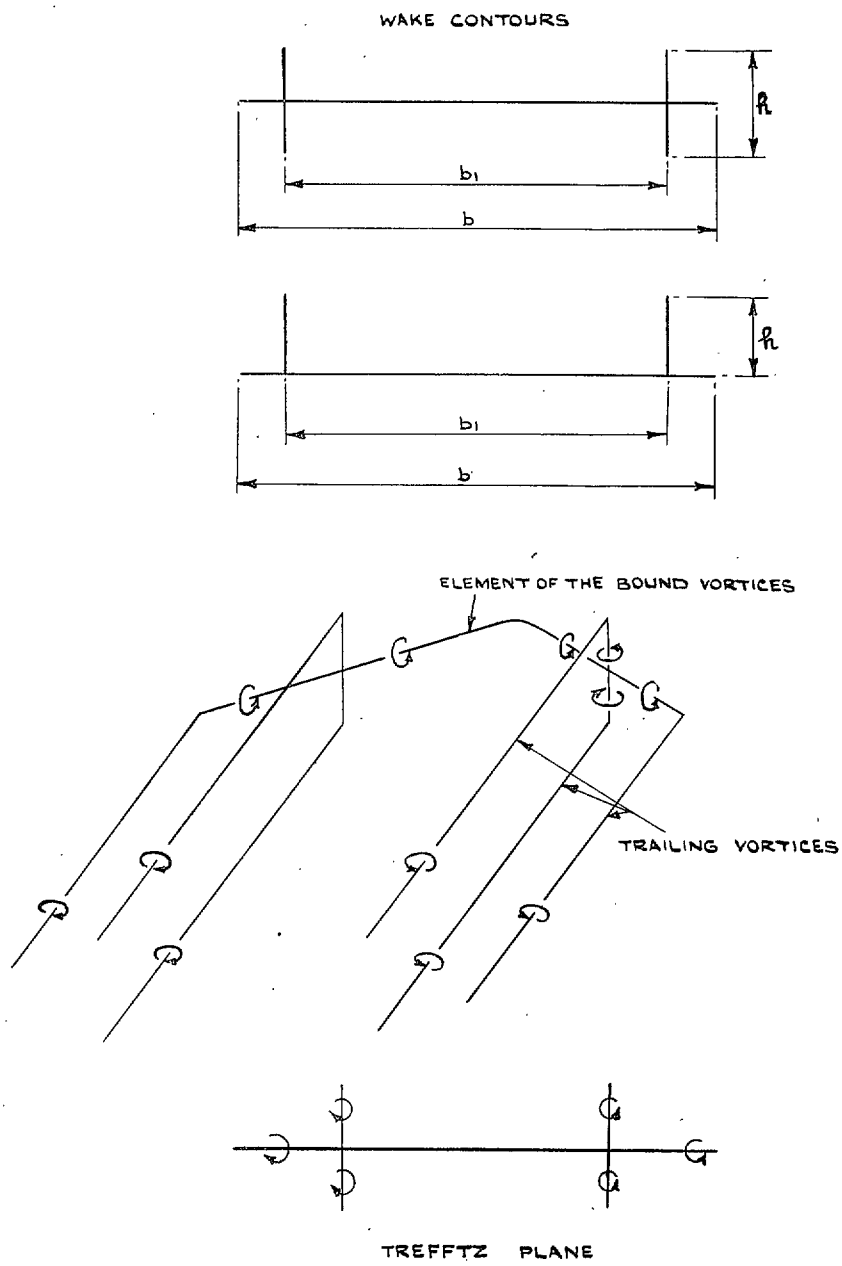

FIG. 1. Nomenclature and vortex system for wing-plate combination.

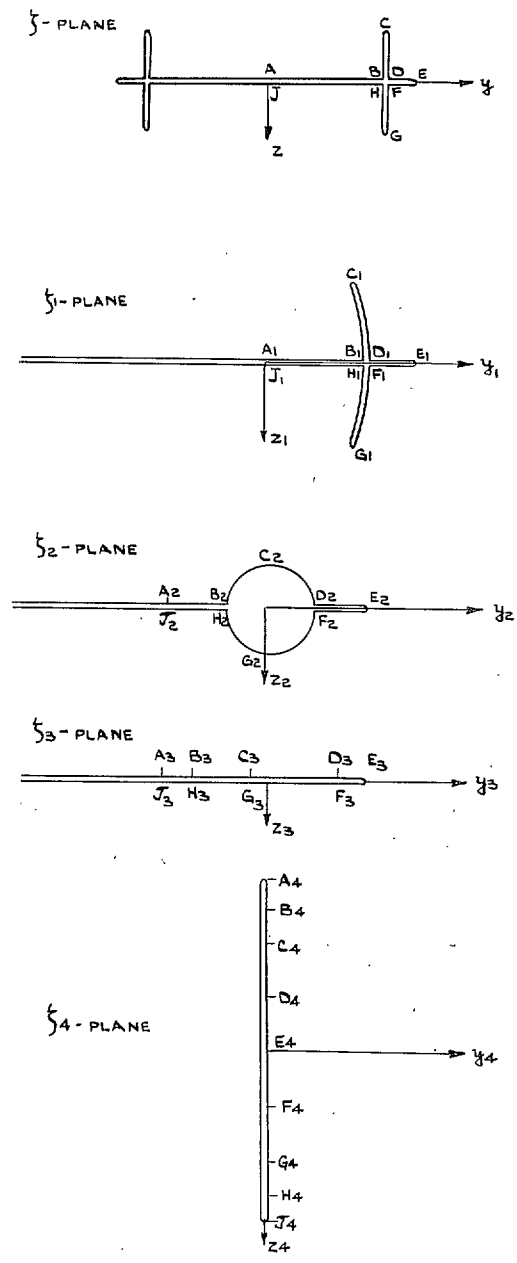

FIG. 2. Sketch of the conformal transformations.

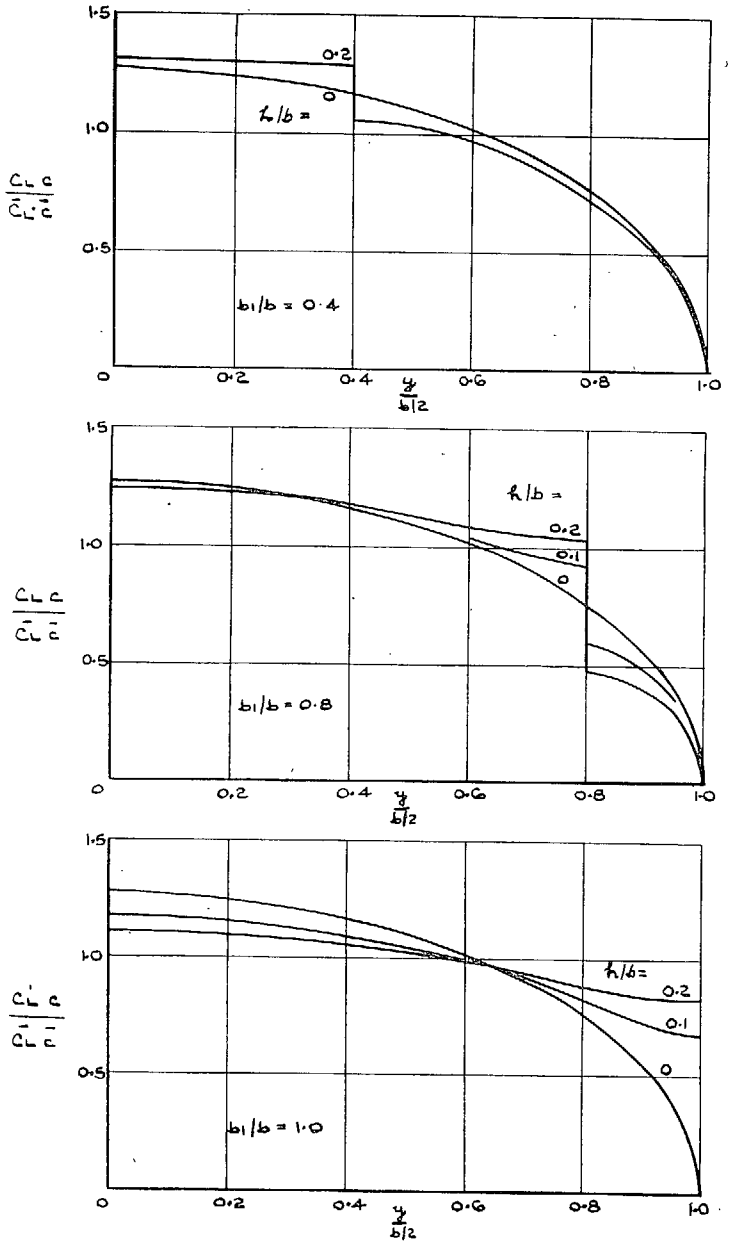

FIG. 3. Spanwise load distributions with plates of equal height above and below the wing.

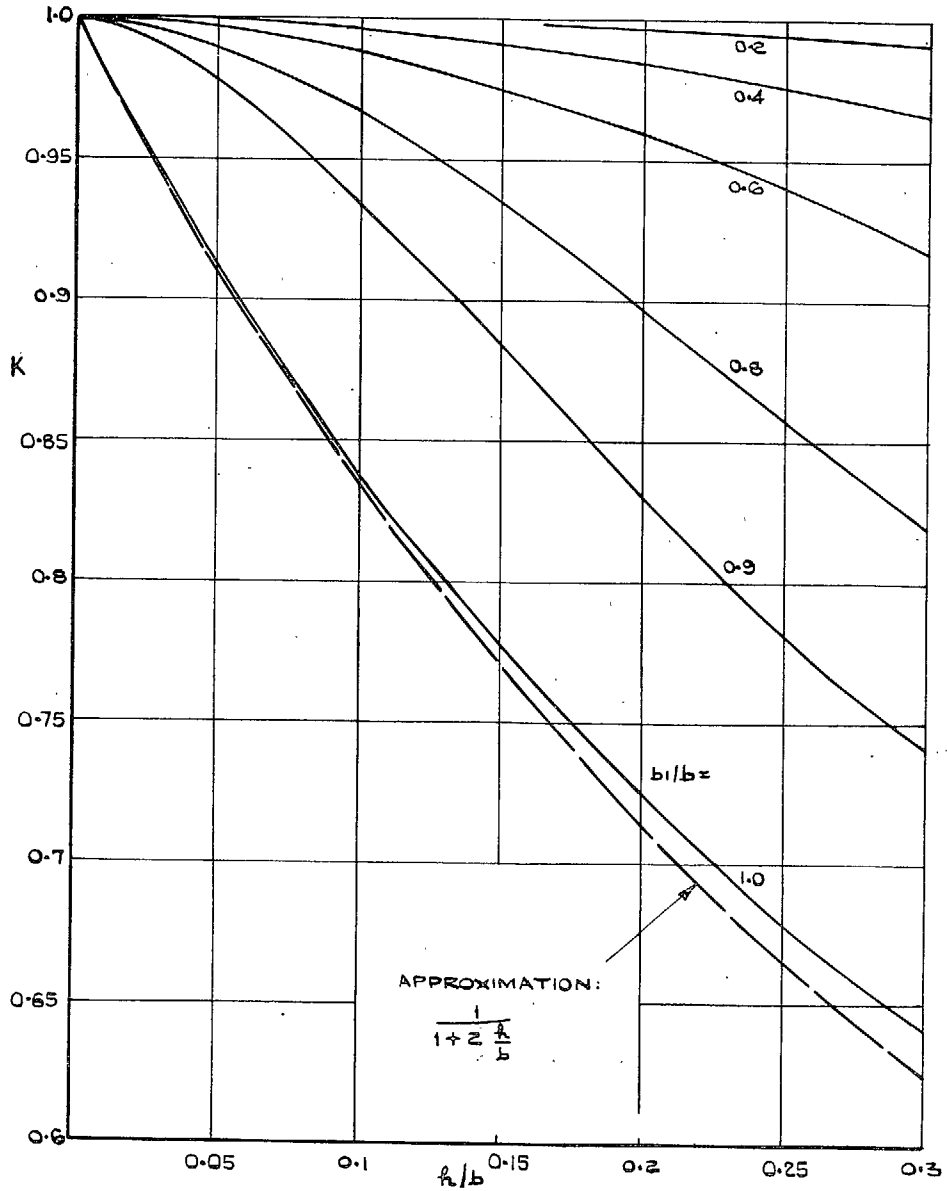

FIG. 4. $\varkappa$-values for plates of equal height above and below the wing.

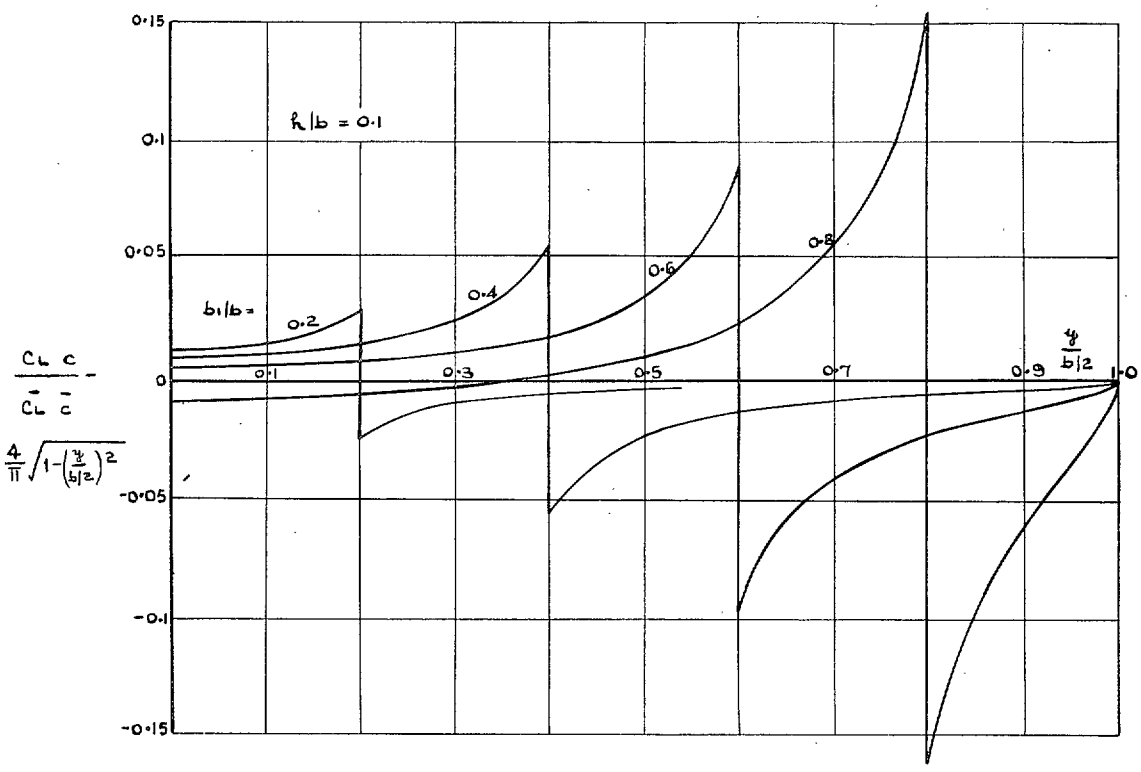

FIG. 5. Additional load distributions. Plates of equal height above and below the wing.

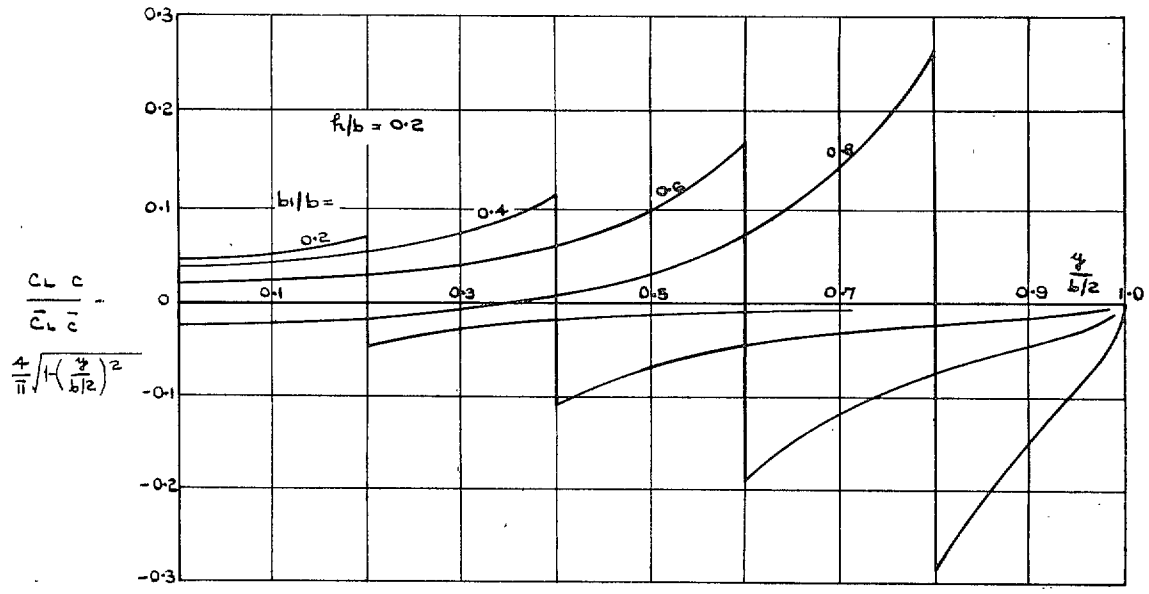

FIG. 6. Additional load distributions. Plates of equal height above and below the wing.

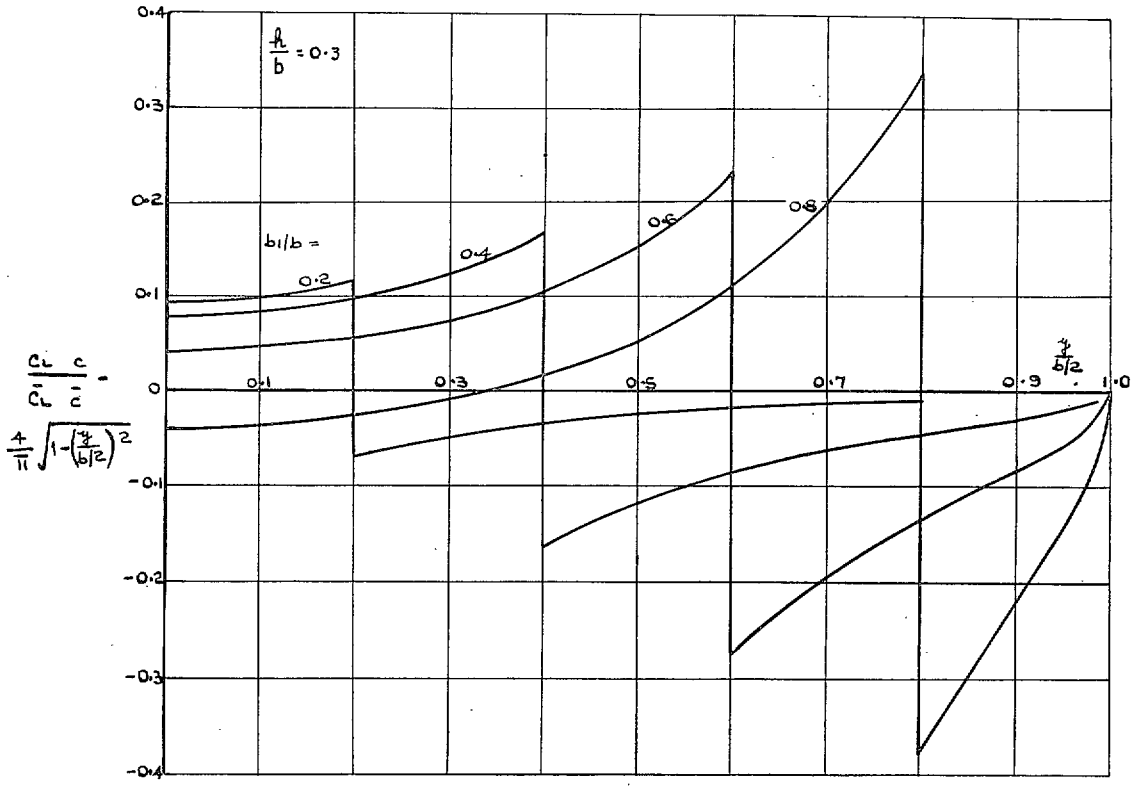

FIG. 7. Additional load distributions. Plates of equal height above and below the wing.

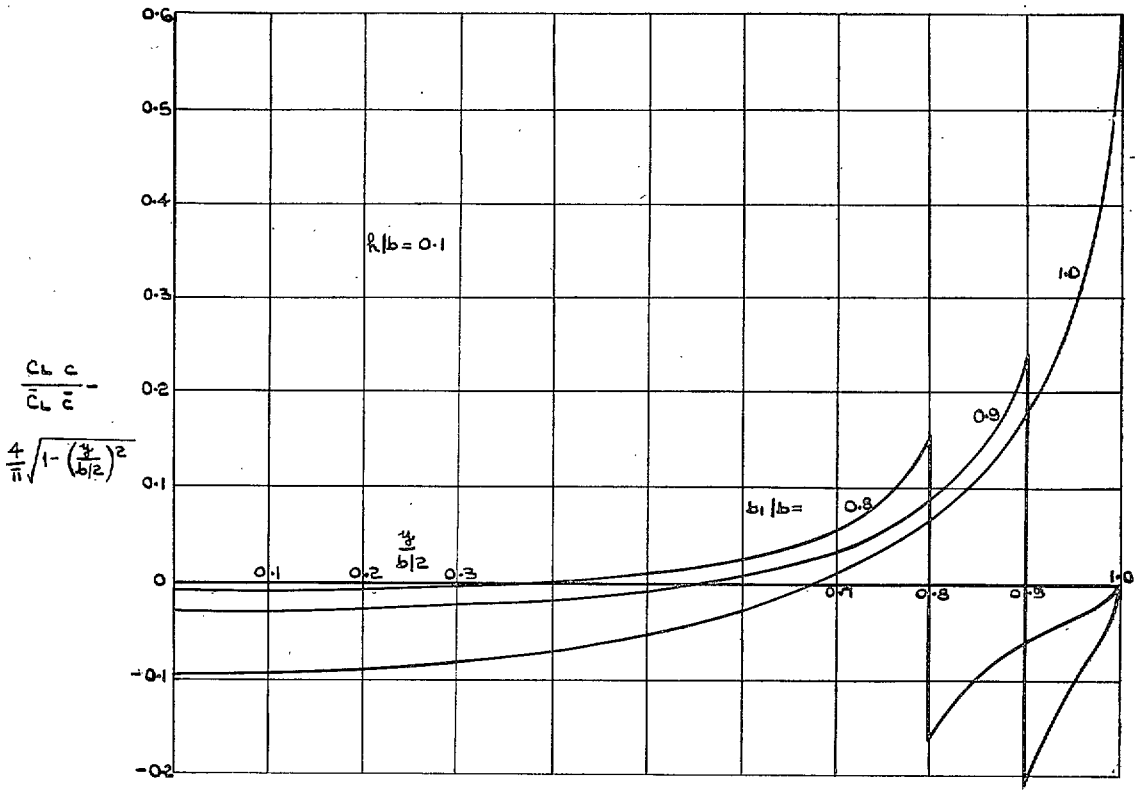

FIG. 8. Additional load distributions. Plates of equal height above and below the wing.

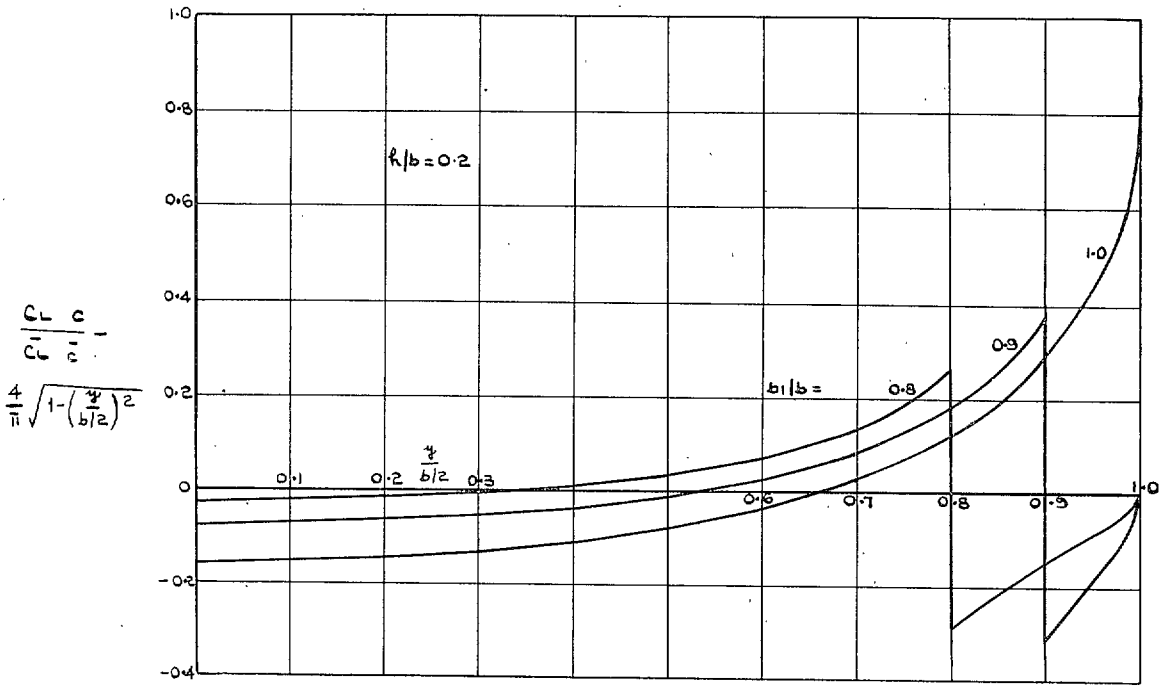

FIG. 9. Additional load distributions. Plates of equal height above and below the wing.

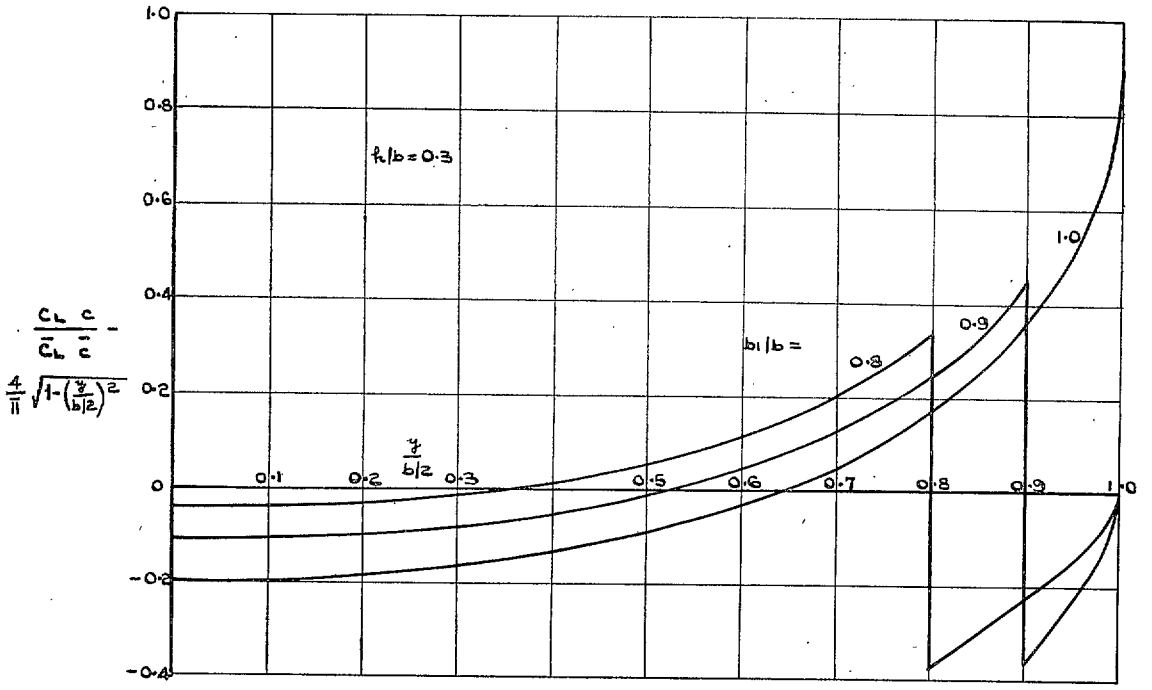

FIG. 10. Additional load distributions. Plates of equal height above and below the wing.

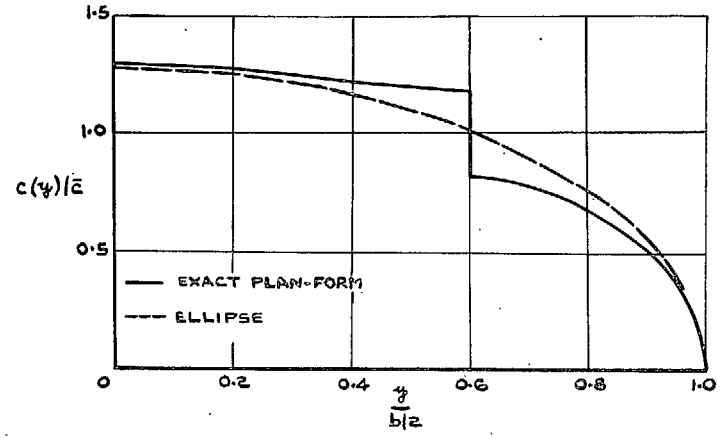

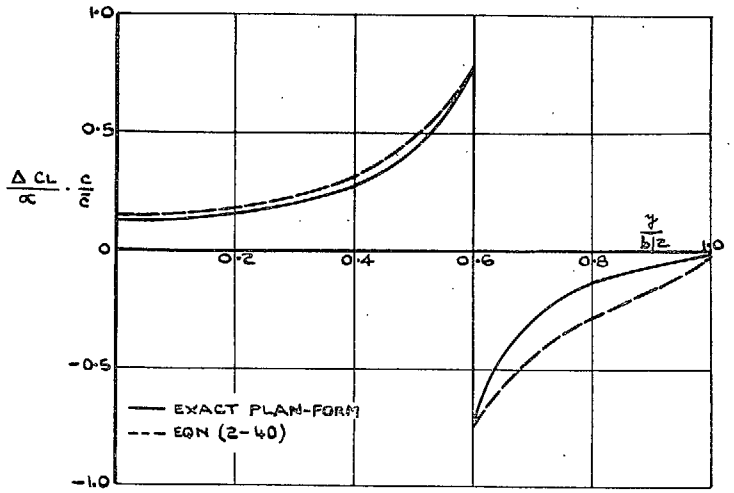

FIG. 11. Plan-form and additional load distribution on wing with plates of equal height above and below the wing

$h/b = 0{\cdot}2$, $b_1/b = 0{\cdot}6$,
A $= 4$, $\varphi = 0$, $a = 2\pi$

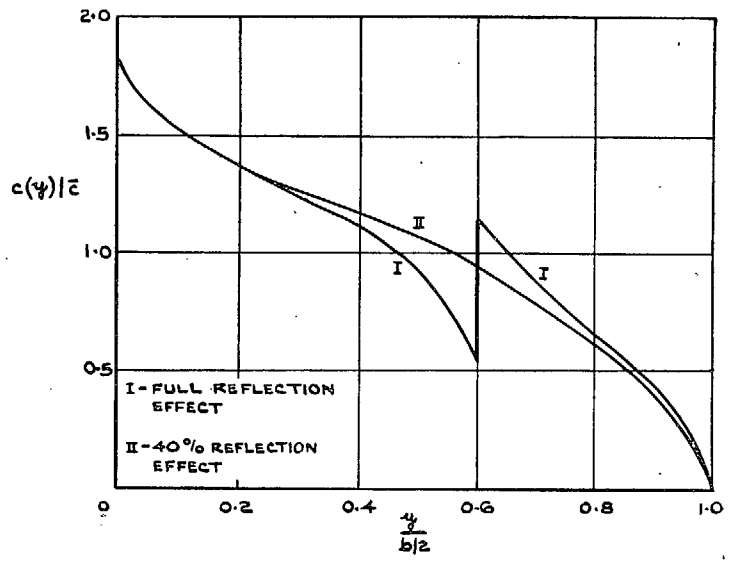

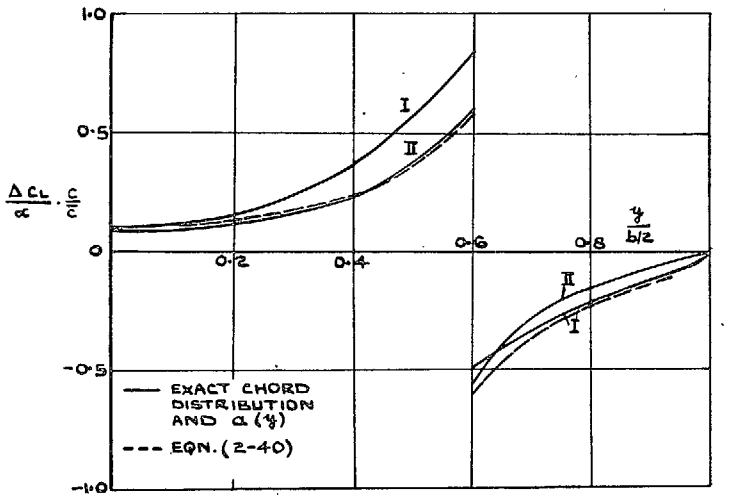

FIG. 12. Chord distribution and additional load distribution on wing with plates of equal height above and below the wing

$h/b = 0{\cdot}2$, $b_1/b = 0{\cdot}6$,
A $= 4$, $\varphi = 45°$, $a_0 = 2\pi$

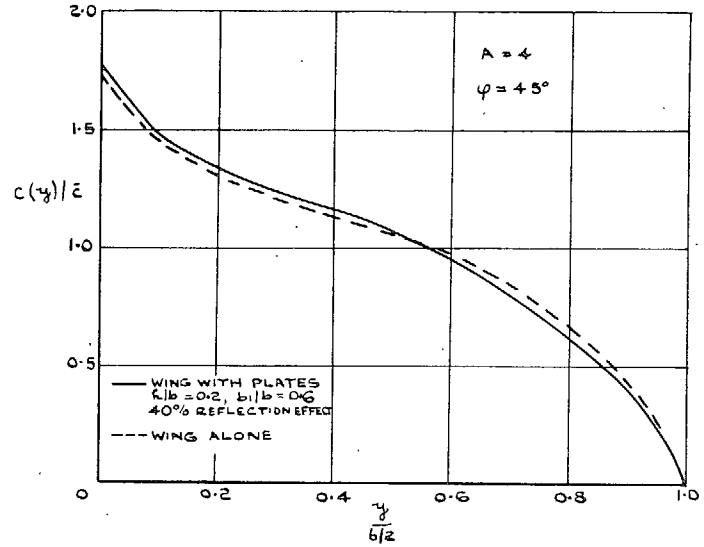

FIG. 13. Chord distributions of minimum induced-drag configurations.

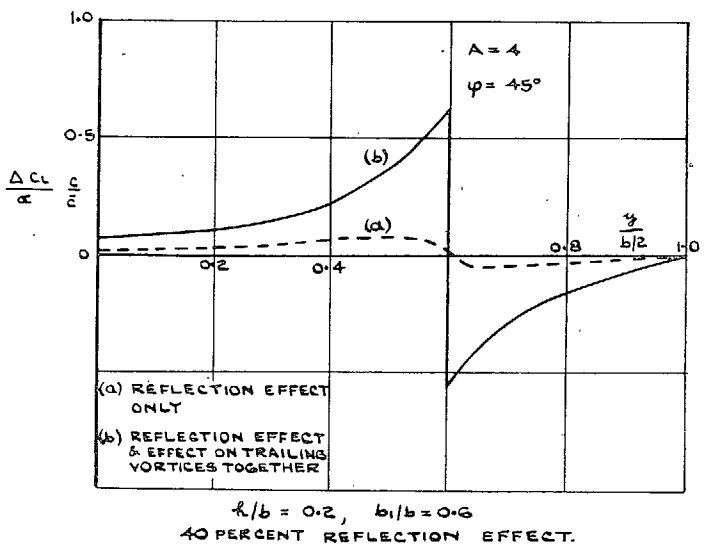

FIG. 14. Additional load distributions on wing with plates of equal height above and below the wing.

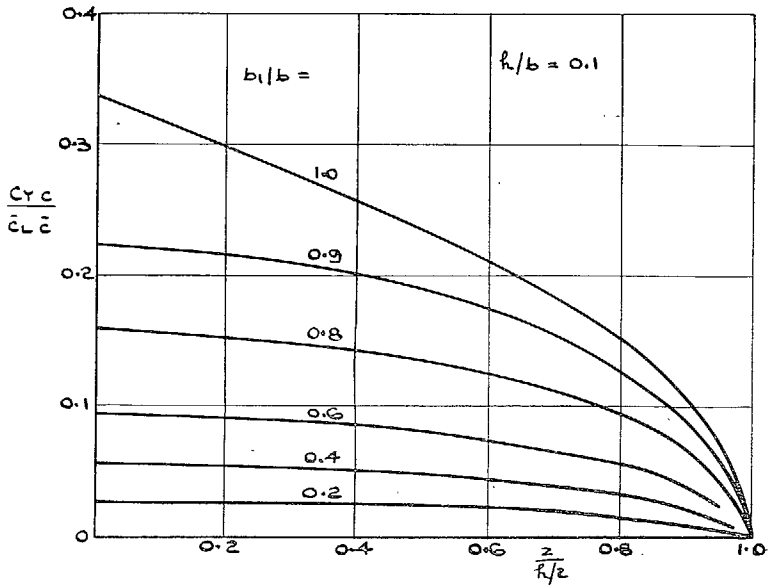

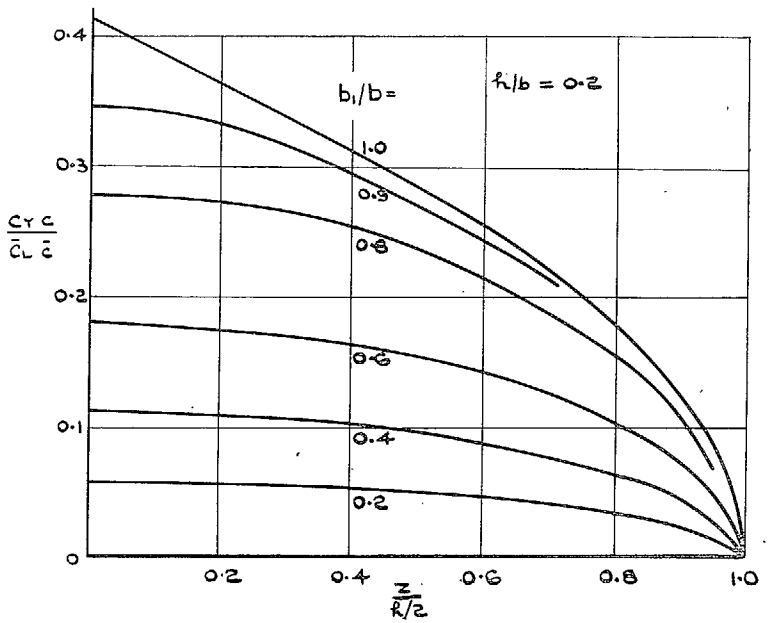

FIG. 15. Side-force distributions. Plates of equal height above and below the wing.

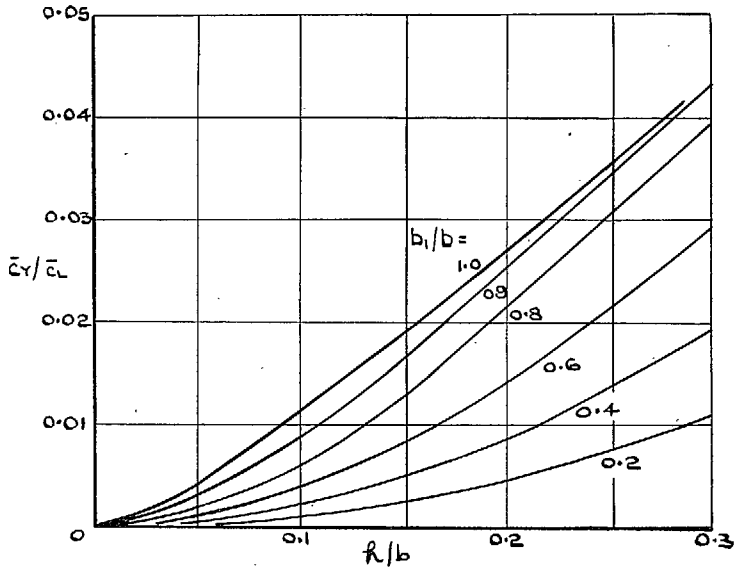

FIG. 16. Total side-force on upper part of a plate. Plates of equal height above and below the wing.

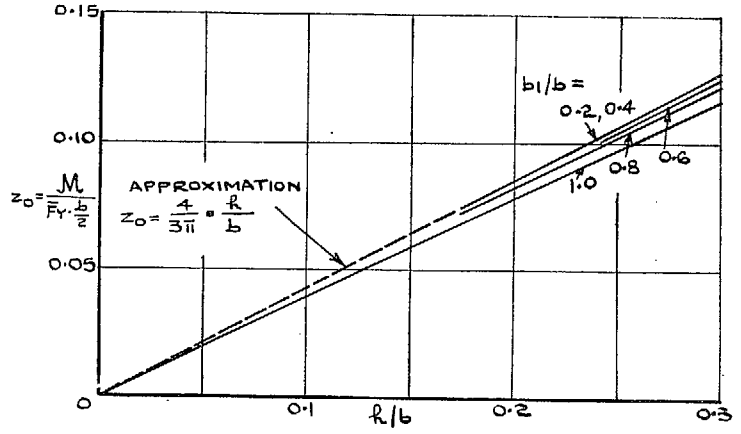

FIG. 17. Moment arm of side-force. Plates of equal height above and below the wing.

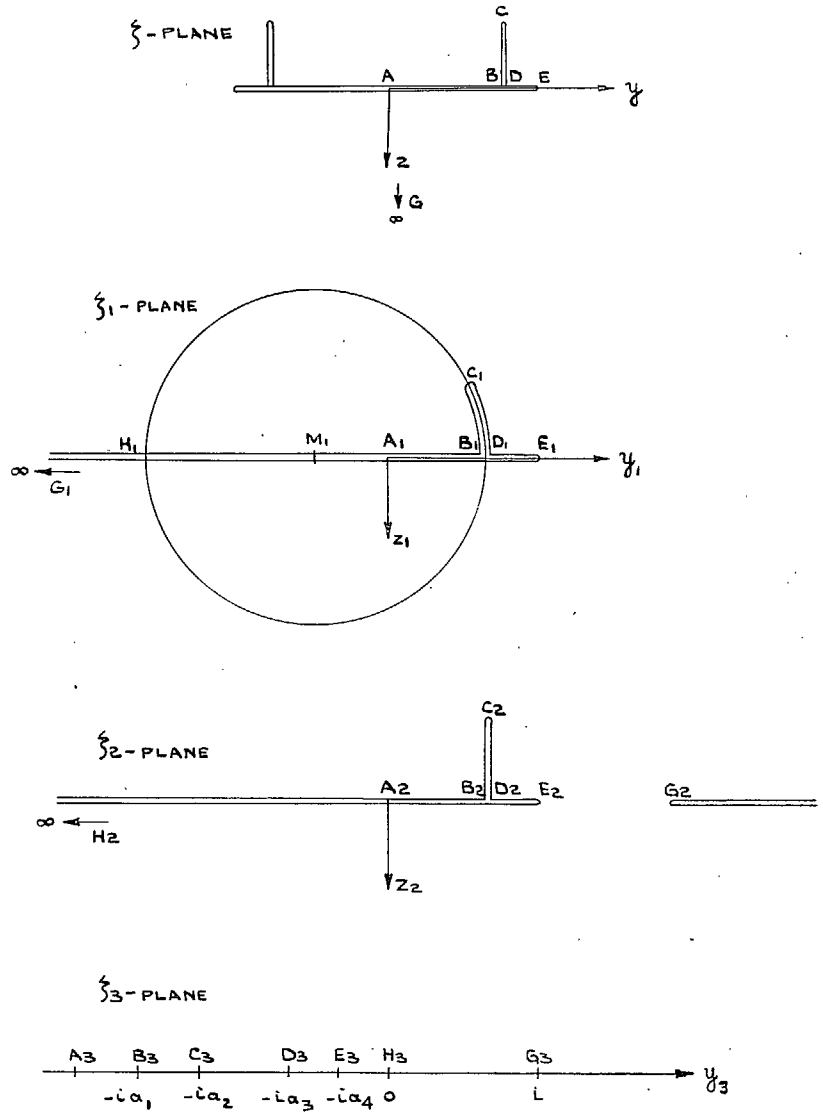

FIG. 18. Sketch of conformal transformations.

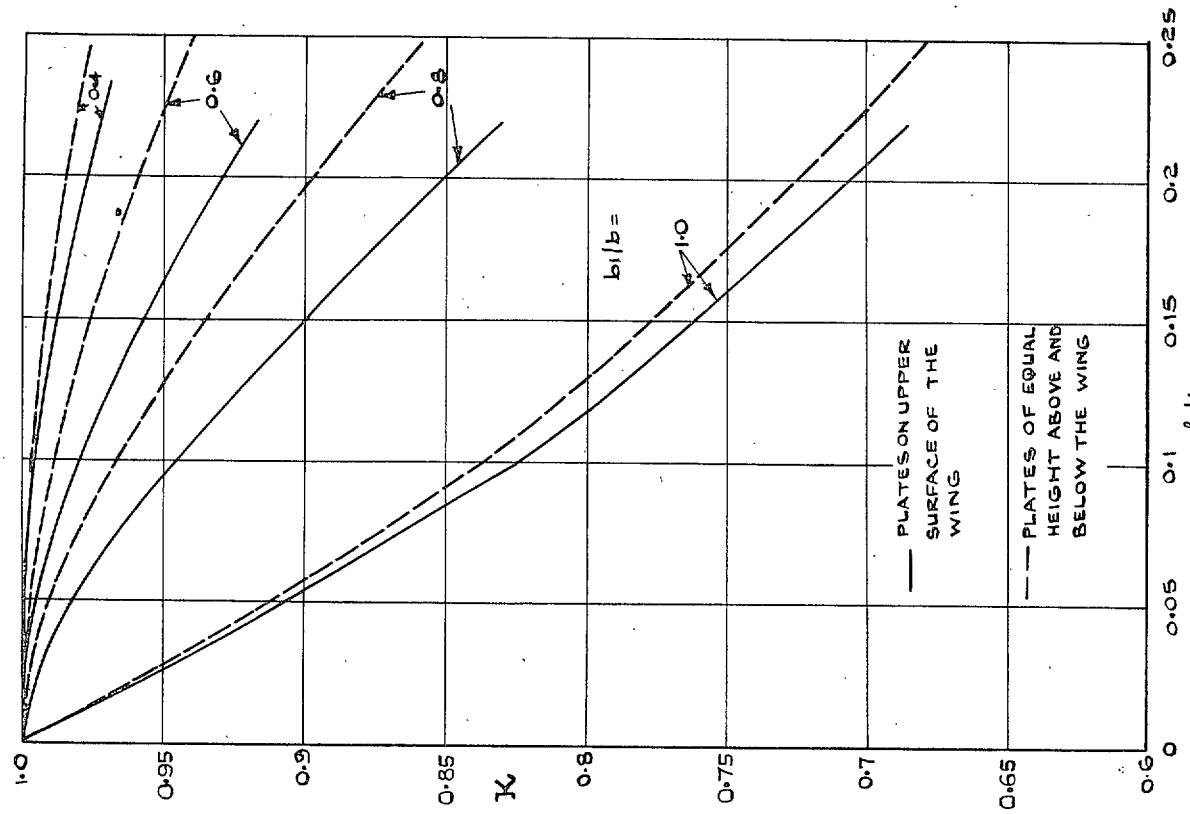

FIG. 19. κ-values.

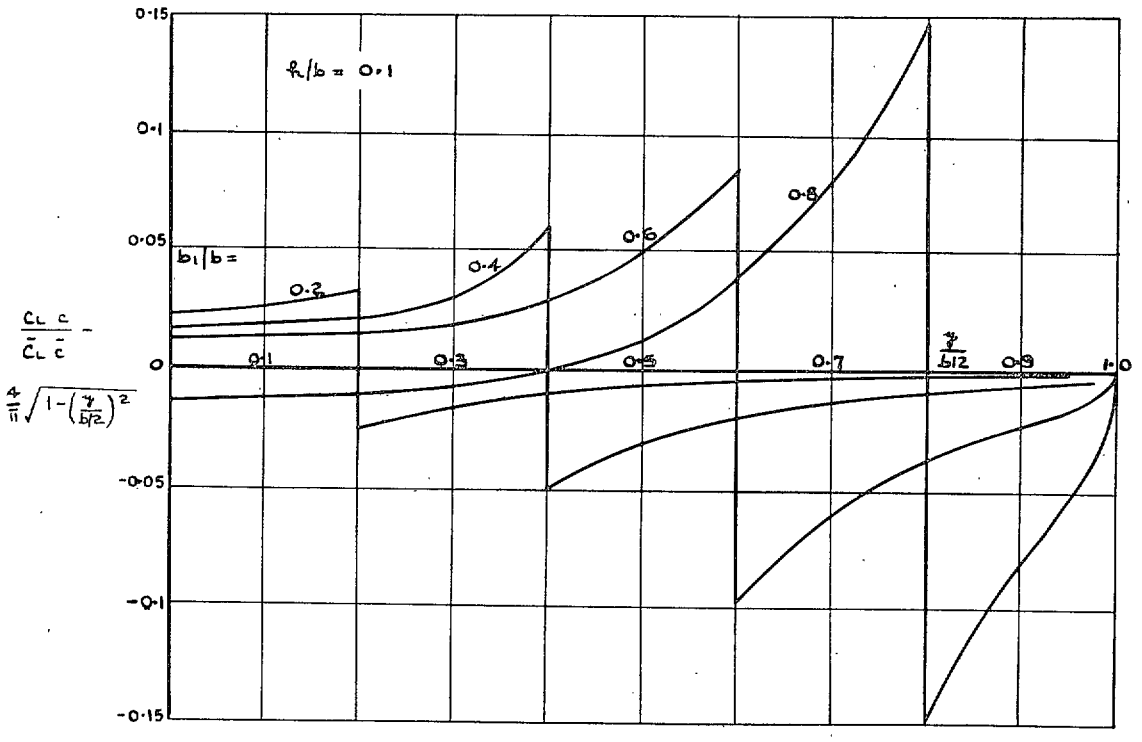

FIG. 20. Additional load distributions. Plates on upper surface of wing.

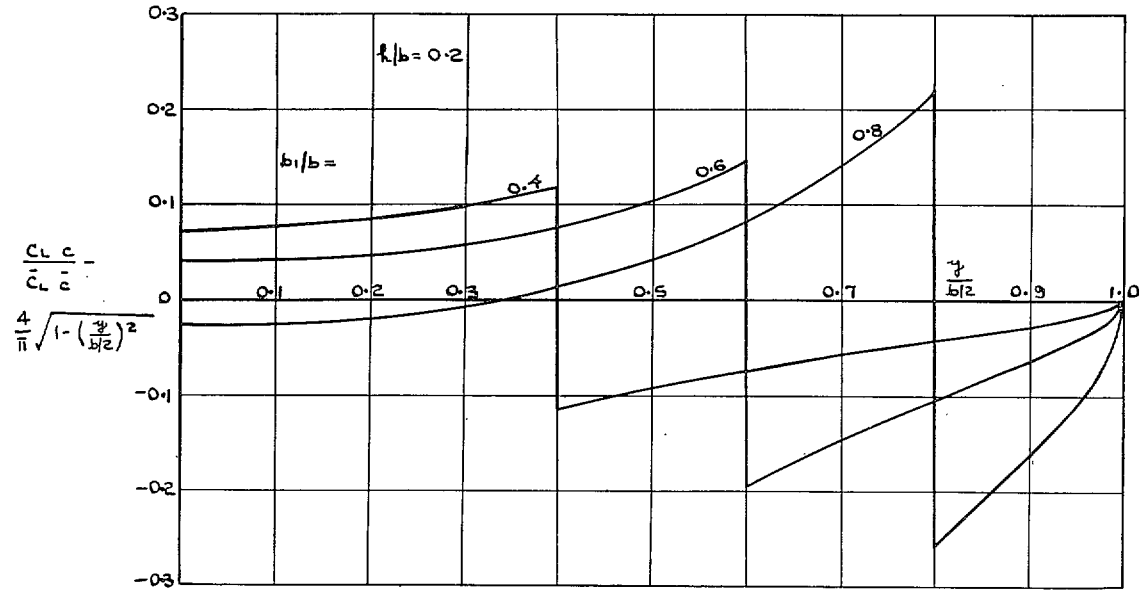

FIG. 21. Additional load distributions. Plates on upper surface of wing.

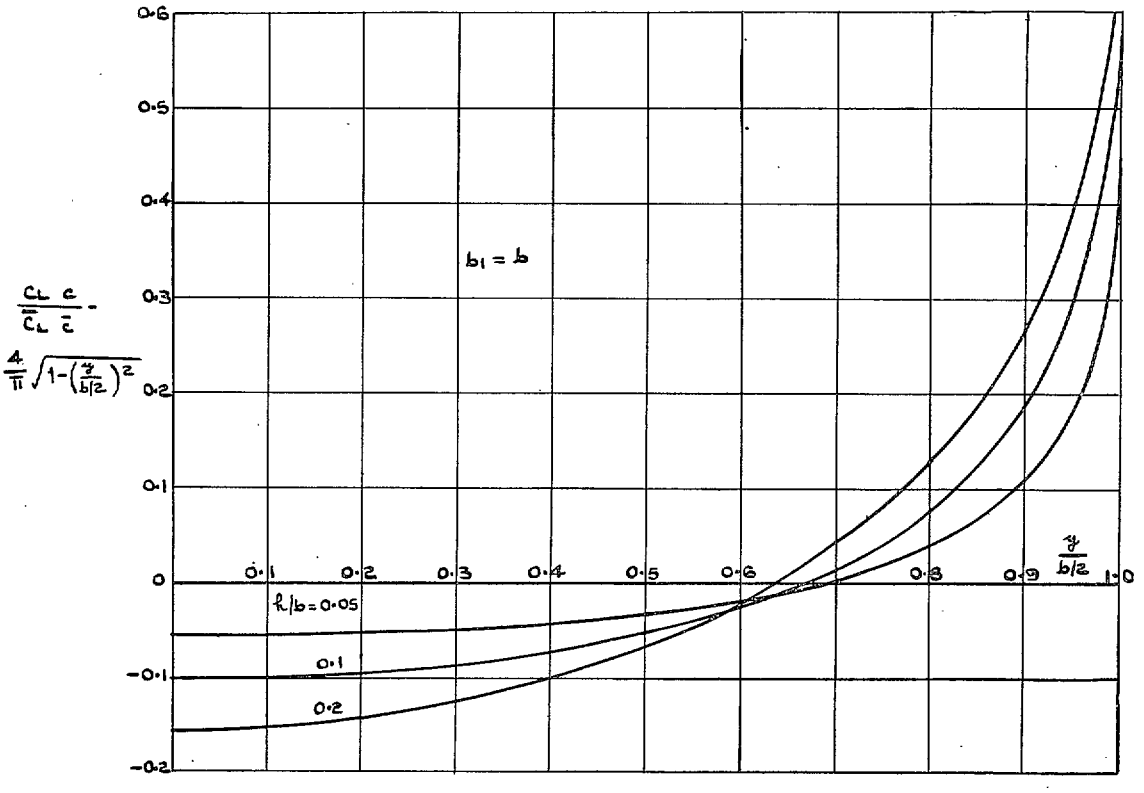

FIG. 22. Additional load distributions. Plates on upper surface of wing.

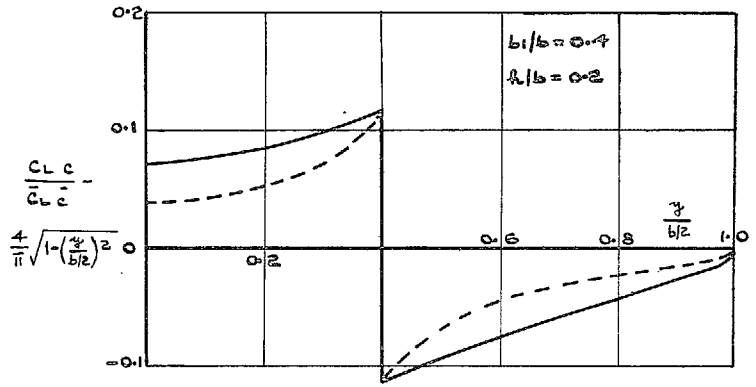

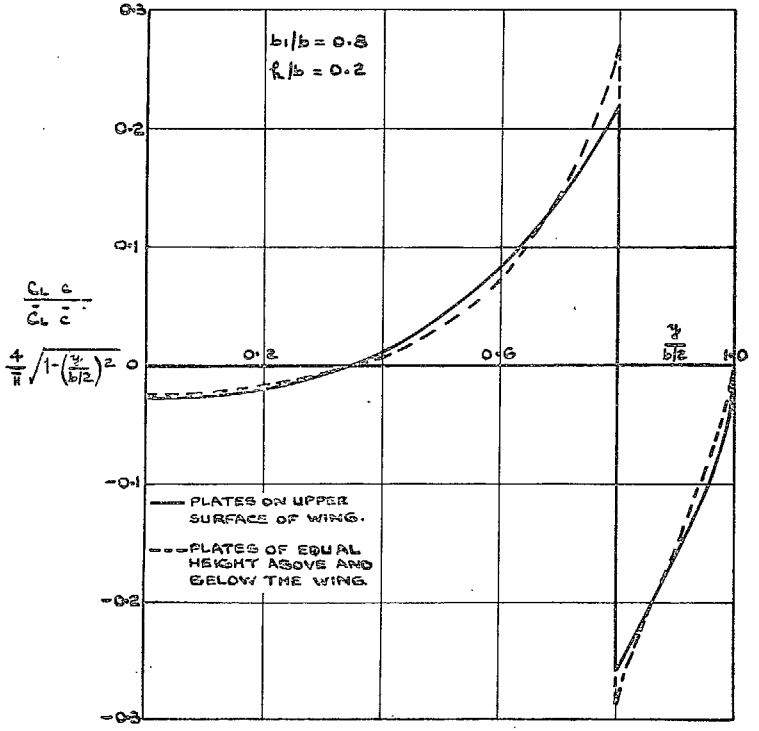

FIG. 23. Additional load distributions.

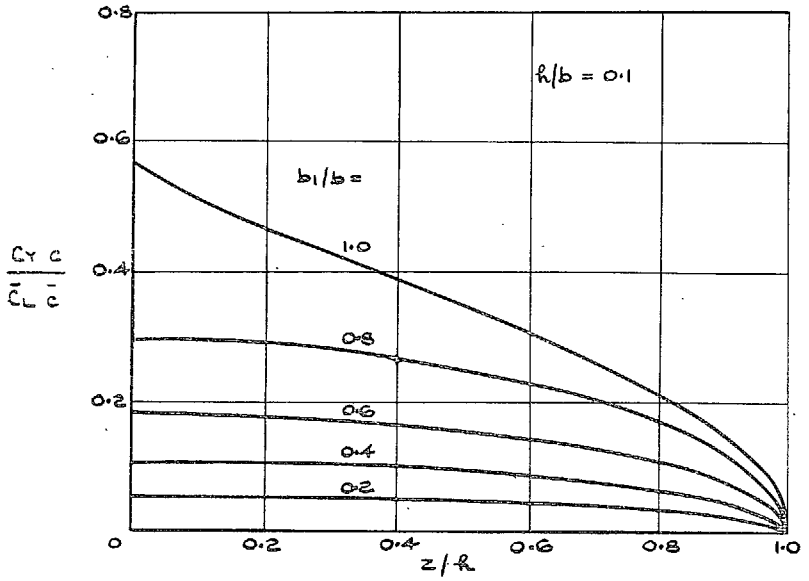

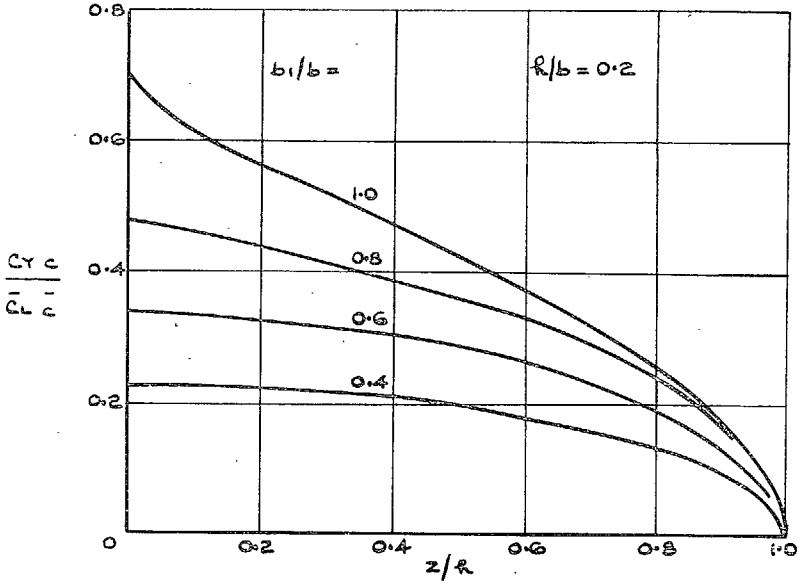

FIG. 24. Side-force distributions. Plates on upper surface of wing.

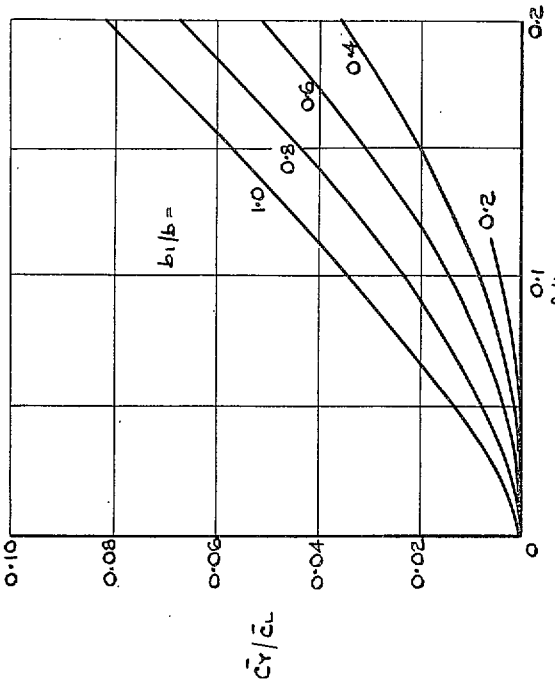

FIG. 25. Total side-force on plate. Plates on upper surface of wing.

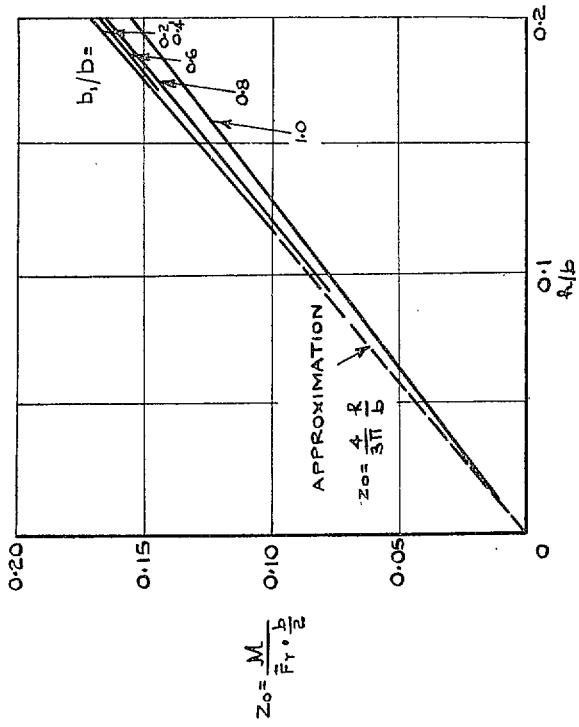

FIG. 26. Moment arm of side-force. Plates on upper surface of wing.

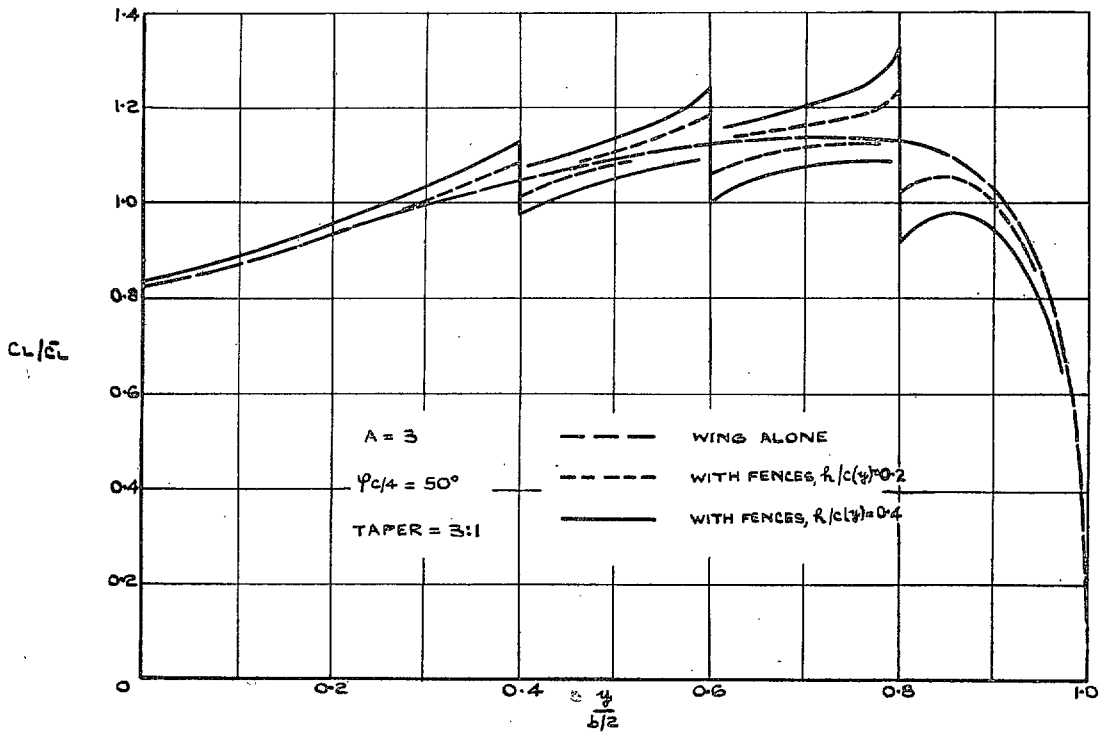

FIG. 27. Lift distributions on wing with fences.

(42880) Wt. 19/8417 K7. 11/56 Hw

PRINTED IN GREAT BRITAIN

Publications of the Aeronautical Research Council

ANNUAL TECHNICAL REPORTS OF THE AERONAUTICAL RESEARCH COUNCIL (BOUND VOLUMES)

1939 Vol. I. Aerodynamics General, Performance, Airscrews, Engines. 50*s.* (51*s.* 9*d.*).
Vol. II. Stability and Control, Flutter and Vibration, Instruments, Structures, Seaplanes, etc. 63*s.* (64*s.* 9*d.*)

1940 Aero and Hydrodynamics, Aerofoils, Airscrews, Engines, Flutter, Icing, Stability and Control Structures, and a miscellaneous section. 50*s.* (51*s.* 9*d.*)

1941 Aero and Hydrodynamics, Aerofoils, Airscrews, Engines, Flutter, Stability and Control Structures. 63*s.* (64*s.* 9*d.*)

1942 Vol. I. Aero and Hydrodynamics, Aerofoils, Airscrews, Engines. 75*s.* (76*s.* 9*d.*)
Vol. II. Noise, Parachutes, Stability and Control, Structures, Vibration, Wind Tunnels. 47*s.* 6*d.* (49*s.* 3*d.*)

1943 Vol. I. Aerodynamics, Aerofoils, Airscrews. 80*s.* (81*s.* 9*d.*)
Vol. II. Engines, Flutter, Materials, Parachutes, Performance, Stability and Control, Structures. 90*s.* (92*s.* 6*d.*)

1944 Vol. I. Aero and Hydrodynamics, Aerofoils, Aircraft, Airscrews, Controls. 84*s.* (86*s.* 3*d.*)
Vol. II. Flutter and Vibration, Materials, Miscellaneous, Navigation, Parachutes, Performance, Plates and Panels, Stability, Structures, Test Equipment, Wind Tunnels. 84*s.* (86*s.* 3*d.*)

1945 Vol. I. Aero and Hydrodynamics, Aerofoils. 130*s.* (132*s.* 6*d.*)
Vol. II. Aircraft, Airscrews, Controls. 130*s.* (132*s.* 6*d.*)
Vol. III. Flutter and Vibration, Instruments, Miscellaneous, Parachutes, Plates and Panels, Propulsion. 130*s.* (132*s.* 3*d.*)
Vol. IV. Stability, Structures, Wind Tunnels, Wind Tunnel Technique. 130*s.* (132*s.* 3*d.*)

Annual Reports of the Aeronautical Research Council—

1937 2*s.* (2*s.* 2*d.*) 1938 1*s.* 6*d.* (1*s.* 8*d.*) 1939–48 3*s.* (3*s.* 3*d.*)

Index to all Reports and Memoranda published in the Annual Technical Reports, and separately—

April, 1950 - - - - R. & M. 2600 2*s.* 6*d.* (2*s.* 8*d.*)

Author Index to all Reports and Memoranda of the Aeronautical Research Council—

1909—January, 1954 R. & M. No. 2570 15*s.* (15*s.* 6*d.*)

Indexes to the Technical Reports of the Aeronautical Research Council—

December 1, 1936—June 30, 1939	R. & M. No. 1850	1*s.* 3*d.* (1*s.* 5*d.*)
July 1, 1939—June 30, 1945	R. & M. No. 1950	1*s.* (1*s.* 2*d.*)
July 1, 1945—June 30, 1946	R. & M. No. 2050	1*s.* (1*s.* 2*d.*)
July 1, 1946—December 31, 1946	R. & M. No. 2150	1*s.* 3*d.* (1*s.* 5*d.*)
January 1, 1947—June 30, 1947	R. & M. No. 2250	1*s.* 3*d.* (1*s.* 5*d.*)

Published Reports and Memoranda of the Aeronautical Research Council—

Between Nos. 2251–2349	R. & M. No. 2350	1*s.* 9*d.* (1*s.* 11*d.*)
Between Nos. 2351–2449	R. & M. No. 2450	2*s.* (2*s.* 2*d.*)
Between Nos. 2451–2549	R. & M. No. 2550	2*s.* 6*d.* (2*s.* 8*d.*)
Between Nos. 2551–2649	R. & M. No. 2650	2*s.* 6*d.* (2*s.* 8*d.*)

Prices in brackets include postage

HER MAJESTY'S STATIONERY OFFICE

York House, Kingsway, London W.C.2; 423 Oxford Street, London W.1 (Post Orders: P.O. Box 569, London S.E.1)
13a Castle Street, Edinburgh 2; 39 King Street, Manchester 2; 2 Edmund Street, Birmingham 3; 109 St. Mary Street, Cardiff; Tower Lane, Bristol, 1; 80 Chichester Street, Belfast, *or through any bookseller.*

S.O. Code No. 23-2960